

**CONSTRUCTION AND
CHARACTERIZATION OF A
FARNSWORTH-HIRSCH FUSOR**

By

Ian J. Love

A thesis submitted in partial fulfillment of the
requirements for the degree of

Bachelor of Science

Houghton College

May 2014

Signature of Author.....

Department of Physics
May 6, 2014

.....

Dr. Mark Yuly
Professor of Physics
Research Supervisor

.....

Dr. Brandon Hoffman
Associate Professor of Physics

**CONSTRUCTION AND
CHARACTERIZATION OF A
FARNSWORTH-HIRSCH
FUSOR**

By

Ian J. Love

Submitted to the Department of Physics
on May 6, 2014 in partial fulfillment of the
requirement for the degree of
Bachelor of Science

Abstract

A table-top Inertial Electrostatic Confinement (IEC) Fusion device was constructed at Houghton College to explore the properties of plasmas and the nuclear reactions that may be induced in this device. A spherical stainless steel wire grid 7.0 cm in diameter mounted centrally in the cylindrical 0.3 m diameter vacuum vessel was raised to nearly 30 kV. A grounded spherical wire grid 20.3 cm in diameter surrounded the charged sphere. An air-cooled oil diffusion pump and a mechanical forepump evacuated the chamber to approximately 10^{-6} Torr. An ion source gas was leaked into the chamber raising the pressure to 1×10^{-3} to 1×10^{-4} Torr. The voltage across the inner grid, the current through the high voltage circuit, the chamber pressure, and the radiation were measured over the course of the experiment. The operation of this device with air as the ion source gas produced x-rays which, passing through a single layer Mylar (BoPET) foil window, were in excess of 400 mR/hr at 0.6 meters from the aperture.

Thesis Supervisor: Dr. Mark Yuly
Title: Professor of Physics

TABLE OF CONTENTS

Chapter 1 Introduction.....	6
1.1 What is Nuclear Fusion?	6
1.2 History	9
1.2.1 Multipactor.....	9
1.2.2 Equations of Motion for an Ideal Plasma	10
1.2.3 Criteria for a Power Producing Thermonuclear Reactor	11
1.2.4 On the Inertial-Electrostatic Confinement of a Plasma	12
1.2.5 1962 Farnsworth Patent.....	12
1.2.6 1968 Hirsch Patent	13
1.3 Motivation	16
Chapter 2 Theory	17
2.1 Equations of Motion for Plasma	17
2.1.1 Simplest Case: Motion of charged particles in \vec{E} and \vec{B} fields	17
2.1.2 Exact Kinetic Plasma Equation	18
2.1.3 Numerical Approximation for Kinetic Plasma Equations.....	22
2.1.4 Averaging the Klimontovich Equation.....	24
2.2 Lawson’s Criterion for Fusion	26
2.2.1 Premise of Criteria	26
2.2.2 Systems in Which the Reaction Products are Retained	27
Chapter 3 Experiment & Apparatus.....	28
3.1 Experimental overview	28
3.2 Vacuum System.....	28
3.2.1 Vacuum pumps and cold trap	28
3.2.2 Vacuum chamber.....	28
3.2.3 Vacuum leak valves.....	31
3.2.4 Gas Pressure	32
3.3 High Voltage System	32
3.3.1 Wire Grids.....	32
3.3.2 High Voltage Power Supply and Ballast Resistor	34
3.3.3 Safety Shield	35
3.3.4 Voltage and Current	36
3.3.5 Electrode Positioning.....	36
3.4 Radiation Measurements.....	36

3.4.1	X-Ray Measurements	36
3.5	Radiation Safety	37
3.5.1	Application of ALARA.....	37
3.5.2	Implementation of ALARA for this project.....	37
3.5.3	Future Implementation of ALARA for this project	38
Chapter 4	Results & Analysis	39
4.1	Voltage/Current/Pressure Measurement.....	39
4.2	Radiation Measurement	40
4.2.1	Dose Rates.....	40
4.2.2	X-ray Spectra.....	42
4.2.3	Photographs of Fusor operation.....	45
Chapter 5	Conclusions	48
5.1	Conclusions	48
5.2	Future Plans	48
Appendix A	Procedures	50
A.1	Vacuum System.....	50
A.1.1	Vacuum Pump Startup Procedure.....	50
A.1.2	Vacuum Pump Shutdown Procedure	51
A.2	High Voltage System	52
A.2.1	System Startup	52
A.2.2	System Reset (if an overload occurs).....	53
A.2.3	System Shutdown.....	53

TABLE OF FIGURES

Figure 1.1 Plot of average binding energy per nucleon.	7
Figure 1.2 Schematic diagram of a Farnsworth-Hirsch IEC fusion reactor.	9
Figure 1.3 P.T. Farnsworth's multipactor.	10
Figure 1.4 The device proposed by Elmore, et al.	13
Figure 1.5 Farnsworth's electric discharge device	14
Figure 1.6 Hirsch's apparatus for generating fusion reactions	15
Figure 2.1 A diagram of a charged particle in \vec{E} and \vec{B} fields.	18
Figure 3.1 The vacuum system diagram	29
Figure 3.2 The Houghton College Farnsworth-Hirsch fusor.	31
Figure 3.3 A comparison plot of pressure data from the hot and cold ion gauges.	33
Figure 3.4 The fusor electrical diagram.	35
Figure 3.5 High voltage safety shield diagram	36
Figure 4.1 Measured current as a function of voltage	39
Figure 4.2 X-ray dose rate as a function of distance from the aperture	40
Figure 4.3 Technique to measure dosage as a function of perpendicular distance	41
Figure 4.4 Dose rate as a function of perpendicular distance	42
Figure 4.5 ^{241}Am calibration x-ray spectrum	43
Figure 4.6 ^{133}Ba calibration x-ray spectrum	43
Figure 4.7 The x-ray energy calibration curve	44
Figure 4.8 Comparison of x-ray spectra showing attenuation.	44
Figure 4.9 Comparison of x-ray spectra showing decrease of intensity with distance	45
Figure 4.10 Photograph of plasma at 1×10^{-2} Torr.	46
Figure 4.11 Photograph of plasma at 1×10^{-3} Torr.	46
Figure 4.12 Photograph of plasma at 1×10^{-3} Torr.	47
Figure 4.13 Photograph of plasma at 1×10^{-4} Torr.	47
Figure A.1 The Vacuum System diagram.	50
Figure A.2 The Sorensen 230-3/12P R&D high voltage power supply	52

Chapter 1

INTRODUCTION

1.1 What is Nuclear Fusion?

When two atomic nuclei combine to form a larger nucleus, a nuclear fusion reaction has occurred. If the nucleus that was created in the fusion reaction has a greater binding energy per nucleon than the two original nuclei, some energy will be released. The liquid drop model for atomic nuclei predicts the binding energy of nucleons in a nucleus. In this model, nucleons bind to nearest-neighbors in a similar way to molecules of a liquid [1,2]. From this model, the semi-empirical mass formula, or Bethe-Weizsäcker formula is obtained:

$$\frac{B}{A} = a_v - a_s A^{-\frac{1}{3}} - a_c \frac{Z(Z-1)}{A^{\frac{4}{3}}} - a_a \frac{(N-Z)^2}{A^2} - \frac{a_p \delta}{A^{\frac{7}{4}}}. \quad 1.1$$

In this equation, B is the binding energy of the nucleus, A is the number of nucleons, Z is the number of protons, N is the number of neutrons, δ is an odd-even constant arising from the number of protons compared to neutrons, and constants a are proportionality constants. The first term of the formula is the volume term, which is proportional to the volume of the nucleus. The second term is the surface term, which is dependent on $A^{-1/3}$ because the surface area of the nuclei is proportional to $A^{2/3}$. The third term, the coulomb term, is related to the electrostatic repulsion between protons. The fourth term is the asymmetry term, which incorporates the Pauli Exclusion Principle. The final term accounts for spin-coupling of nucleons, and is called the pairing term constant, which accounts for spin-coupling of nucleons. From this equation, it is possible to construct a plot showing how the average binding energy per nucleus changes with the atomic mass number, as in Figure 1.1. The binding energy per nucleon peaks near iron, with an atomic mass of 56. The greatest energy change results from fusion reactions that combine hydrogen nuclei to form helium, since helium is especially stable due to its “doubly magic” number of protons and neutrons, which occurs when both proton and neutron shells

are closed. In fact, due to “magic” proton and neutron numbers that result in greater nuclear stability, peaks can be observed in Figure 1.1 that represent especially stable isotopes such as ${}^4_2\text{He}$, ${}^{16}_8\text{O}$, and ${}^{40}_{20}\text{Ca}$. Figure 1.1 shows that energy is released by fusion of light nuclei and fission of heavy nuclei, and that nuclear reactions of nuclei close to iron in atomic mass release less energy per nucleon.

Due to their positive charge, for nuclei to fuse, it is necessary to overcome the repulsive Coulomb force. To accomplish this with a thermonuclear device, high temperatures and pressures, such as those found in the Sun, are required. This is because high temperatures and pressures increase the interaction rate between nuclei and decrease the distance between particles at closest approach. The fuel must be in the form of a plasma to increase the nucleon velocity and the rate of interaction between nuclei. For this process to be controlled, the plasma ions must be confined, so that the temperature and density can be sufficient for fusion ignition to occur.

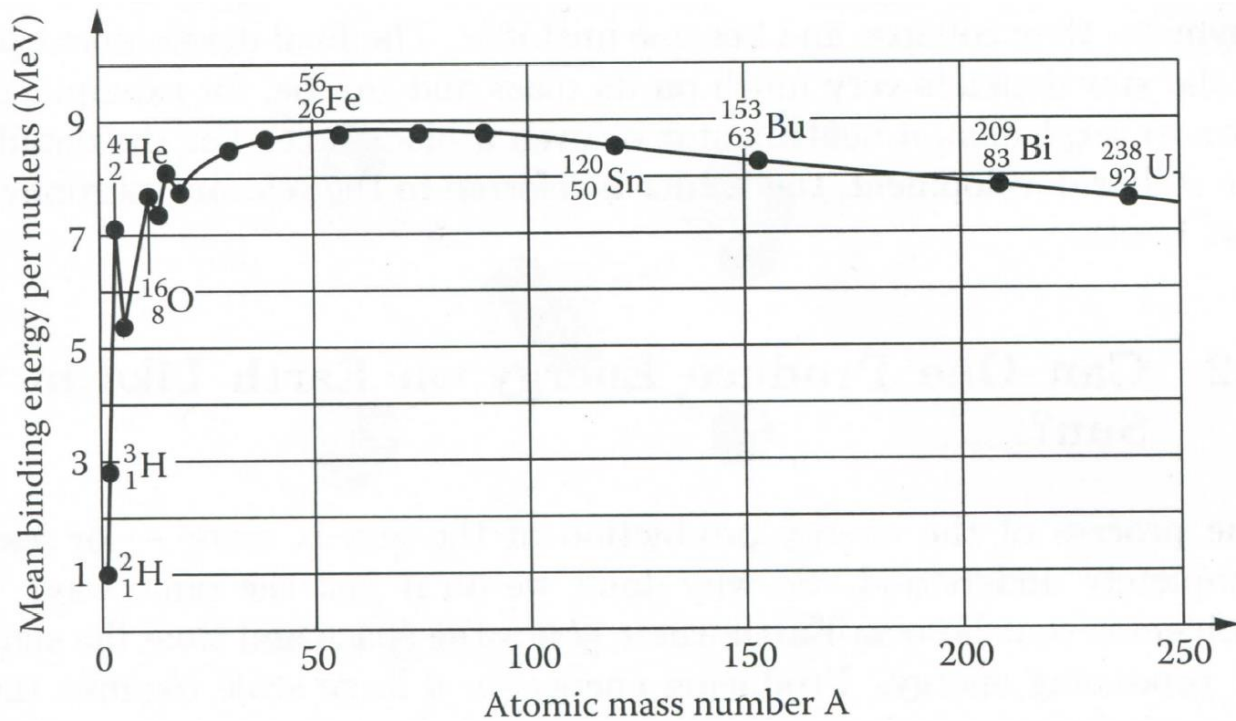


Figure 1.1 The average binding energy per nucleon plotted with respect to the atomic mass number. Peaks due to “magic” numbers of neutrons and protons can be seen at $A=4$ and 16 . Figure obtained from Ref [3].

In order to achieve this confinement, several methods have been devised. In tokamak based fusion reactions, a typically toroidal pressure vessel with a helical magnetic field is used to contain the plasma. In these devices, the helical magnetic fields are generated by electromagnets located on the toroidal pressure vessel which cause charged particles to maintain closed orbits within the tokamak [4]. The plasma remains confined in the tokamak for the comparatively long period of time of several seconds to minutes because the helical magnetic field causes charged particles to orbit in the tokamak in closed orbits. The pressure vessel is evacuated before operation, and then deuterium and tritium fuel is injected into the chamber. When a temperature of approximately 10^8 K is achieved, and a plasma pressure of 5-10 bar is established [5], the magnetic field can be used to control the plasma in the tokamak. The high temperatures required for the fusion reaction are achieved through three different methods of heating: ohmic heating, RF heating, and the injection of beams of high kinetic energy neutral particles, typically deuterium, into the pressure vessel [6]. To obtain these high kinetic energy particles, a particle accelerator accelerates neutral particles, such as deuterium atoms. A current magnetic confinement fusion reactor project is the International Thermonuclear Experimental Reactor (ITER) [7], being built in France as a collaboration between scientists from countries around the world. In this experiment, an attempt is being made to develop magnetically confined fusion reactions to a point where they can be employed as a practical source of heat for generating electricity.

The other methods used to confine the plasma are inertial in nature. In the most commonly used inertial confinement method, called inertial confinement fusion (ICF), lasers, or sometimes charged particle beams, both confine and heat a fuel sample, typically a small spherical pellet of hydrogen isotopes, to initiate a fusion reaction. In contrast with fusion in tokamak magnetic confinement reactors, the typical confinement time for plasma in ICF is much less, on the order of 10^{-10} seconds [8]. Research into ICF is progressing at several laboratories around the world. For example, in the United States at the Lawrence Livermore National Laboratory (LLNL) National Ignition Facility (NIF)[9] and the Laboratory for Laser Energetics (LLE) OMEGA laser [10].

Another inertial confinement method is called inertial electrostatic confinement (IEC) fusion. In this technique, a diffuse fuel gas encounters a negatively charged, typically spherically symmetrical, electrode

grid charged to tens of kilovolts, ionizing the gas in a plasma discharge [11]. The high voltage on the inner grid attracts the ions from the plasma discharge, and accelerates them in orbits towards and around the center of the spherical grid, as in Figure 1.2. If the accelerating voltage is enough, these ions can fuse with other ions or neutral atoms in the plasma.

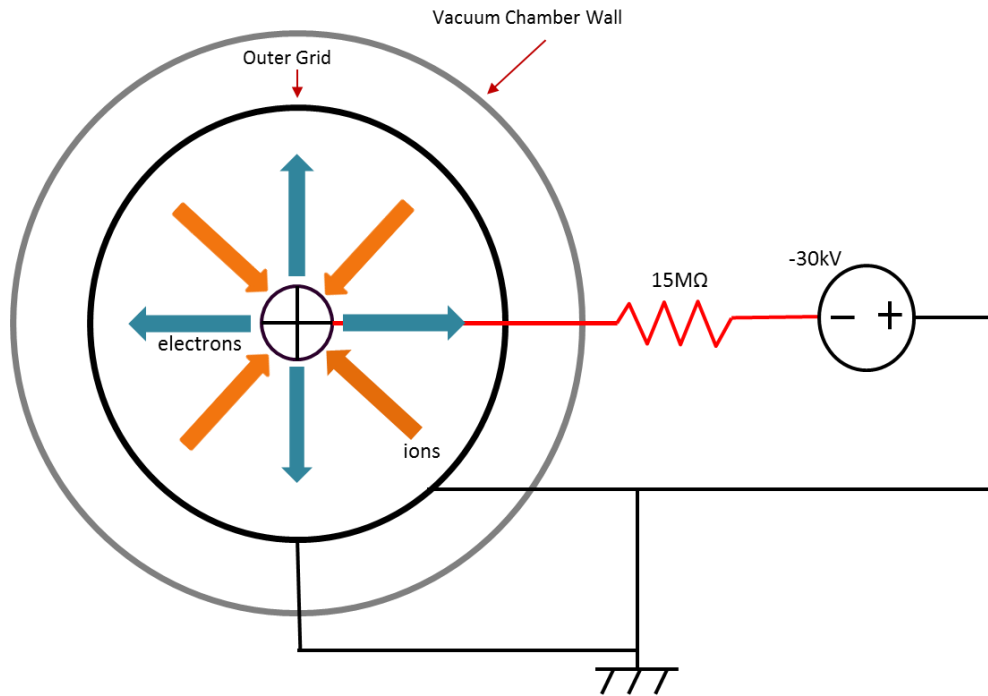


Figure 1.2 Schematic diagram of a Farnsworth-Hirsch type IEC fusion reactor. Positively charged ions are attracted to the “virtual cathode” at the center of the device, and electrons are attracted to the grounded grid and the grounded chamber walls.

1.2 History

1.2.1 *Multipactor*

The early research into IEC fusion technology resulted from vacuum electron tube and the television research. J. Rodney M. Vaughan describes [12] a method of amplifying electric currents through the use of secondary electron emission discovered by Philo T. Farnsworth in 1934. Secondary electron emission is the release of electrons from a metal surface due to impacts by electrons. The multipactor effect is

observed in electron tubes designed to use RF fields to synchronously drive the oscillation of a sheet-like cloud of electrons between two metal surfaces. This discharge builds up and is sustained by secondary emission from the impacts with the surfaces. Vaughn describes how Philo T. Farnsworth discovered [13] the multipactor effect, and how Farnsworth envisaged the use of this device to amplify signals. Farnsworth's multipactor was utilized in early television camera tubes, allowing amplification of light signals. From what Farnsworth learned in his work with multipactor vacuum systems, he reasoned that, with a similar method, ions could be accumulated in a region, which could then interact and fuse. In this way, he was able to develop the idea of the inertial electrostatic confinement fusion device known as the Farnsworth fusor. Figure 1.3 is the interior diagram of the multipactor electron tube developed by Farnsworth in a 1938 patent [14].

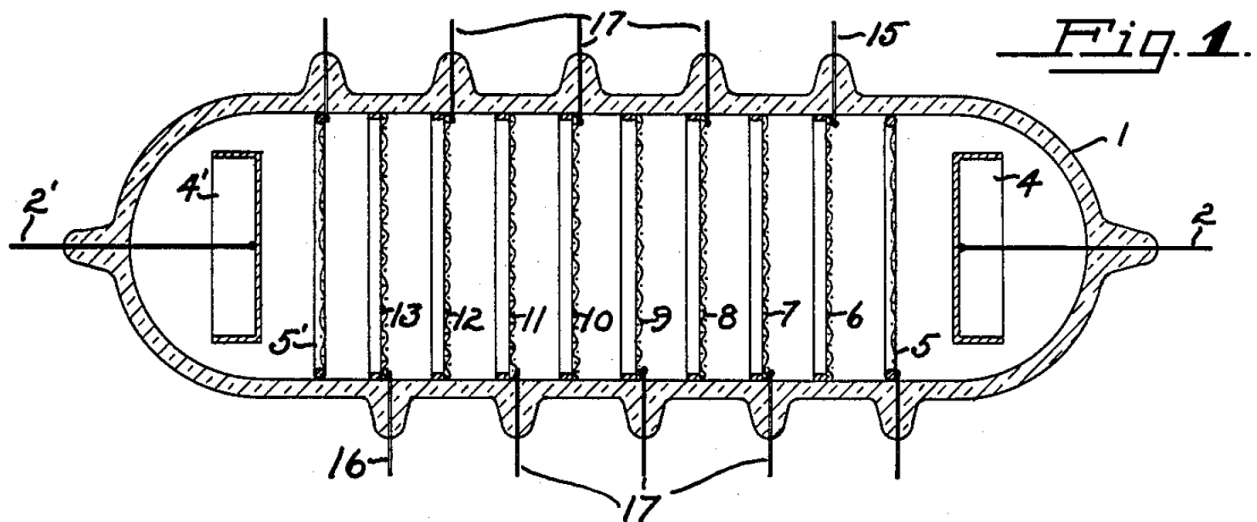


Figure 1.3 P.T. Farnsworth's multipactor, a device that amplifies electric currents through secondary electron emission. Multiple metal plates exist in this device, allowing secondary electron emission in multiple sites. Figure taken from Ref [14].

1.2.2 Equations of Motion for an Ideal Plasma

In order to understand how to confine plasmas for use in fusion reactions, research into the motion of ions in plasma was needed. In 1952, Lyman Spitzer developed equations of motion for an ideal plasma

[15]. Three assumptions are made in the formulation of these equations of motion: (1) the plasma is completely ionized; (2) the macroscopic density and velocity change only very slightly during the time of one gyration of the ion in the magnetic field or over the distance of one radius of gyration of the ion in the magnetic field; and (3) the mean free path between collisions is very great compared to the radius of gyration. If a plasma fulfills these three conditions, it is called an “ideal plasma.” This definition of an ideal plasma is primarily designed for use in the consideration of interstellar plasma, but these equations can also be used in the description of plasmas in other contexts with similar conditions.

1.2.3 *Criteria for a Power Producing Thermonuclear Reactor*

John D. Lawson developed a theory describing the requirements for magnetic and inertial confinement fusion reactor designs in 1956 [16]. He determined that for thermonuclear systems in which the reaction products are retained, for example magnetic confinement fusion, the temperature of the system required for self-sustaining operation in the absence of conduction loss can be found by equating the radiation loss, which is the energy lost due to bremsstrahlung radiation, to the energy carried by the charged reaction products. Lawson determined the temperatures necessary for self-sustaining fusion reaction to be approximately 3×10^8 °C for the D-D reaction, and 5×10^7 °C for the DT reaction. Lawson observed that the D-D reaction is difficult to maintain, since for this reaction temperatures above 10^8 °C cause the reaction rate to increase with temperature only slightly faster than the radiation loss.

For systems in which the reaction products escape, and thus operate on short time scales, Lawson determined that it is possible to ignore conduction loss, and that the energy used to heat the gas and supply energy to the radiation loss is regained to the system as useful heat. Based on the reaction conditions, for a useful D-D fusion reactor with a pulse length of 1 microsecond, it is necessary to attain temperatures above 2×10^8 °C and a pressure of 6×10^8 atmospheres. For a DT fusion reaction in a system in which the reaction products escape, Lawson determined that the conditions necessary for a useful reactor were easier to attain, but still extreme, with a minimum temperature of 3×10^7 °C, with a short confinement time on the order of $1\mu\text{s}$ and high pressures on the order of 6×10^8 atmospheres.

1.2.4 *On the Inertial-Electrostatic Confinement of a Plasma*

In 1959, William C. Elmore, James L. Tuck, and Kenneth M. Watson at Los Alamos Scientific Laboratory proposed a device to confine a plasma through the acceleration of radially projected electrons from a spherical surface [17]. They did not believe this device would be useful as a thermonuclear reactor, but that it would prove of use in the study of thermonuclear plasmas. In this apparatus, a grounded spherically symmetrical conductive shell surrounds a positively charged spherical grid, as in Figure 1.4. Electrons conducted through the grounded shell are emitted toward the center of the device due to the positive potential on a spherical grid concentric with the outer shell. They predicted that these electrons oscillate several times through the center of the device before being captured by the positively charged grid. The optimum conditions for plasma confinement in the experimental system were determined, the thermonuclear economics in these optimum conditions investigated, and the stability of the apparatus was analyzed. They analyzed the system and found that it was unstable for ion densities high enough to produce a significant thermonuclear yield.

1.2.5 *1962 Farnsworth Patent*

Philo T. Farnsworth submitted a patent application in 1962 for the device in Figure 1.5 that used an electric discharge to produce interactions between nuclei [18]. This device used an electric field to oscillate ions at a velocity sufficient to result in nuclear reactions. This invention is “an electron tube structure having concentrically arranged cathode and anode elements, the anode element being electron permeable and supported within the cathode element.”[19] The electrons that are emitted by the cathode go through the anode and reach the center of the device. The “small virtual cathode” created at the center of the device is a consequence of the deceleration of the electrons, which at the point they reach the center, have slowed considerably. The virtual cathode is created by the formation of cloud of electrons in the core of the device. It is called a “virtual cathode” because it is a negatively charged region in the device that comes into existence only when the device is operating. Atoms are ionized through interaction with the electrons in the electron cloud in the virtual cathode. These ions begin to oscillate at nuclear-reaction velocities within the space inside the anode element through the center of the device due to the forces of the electrical potential in this region. Ions accelerated in this way interact to produce nuclear reactions.

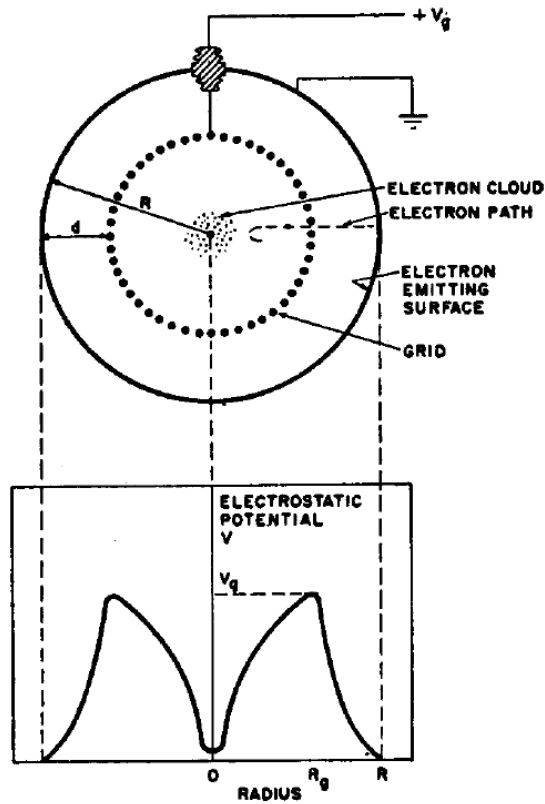


Figure 1.4 The device proposed by Elmore, et al. In this device, electrons are attracted to the positively charged grid, and form an electron cloud in the center of the device. Figure taken from Ref [18].

1.2.6 1968 Hirsch Patent

As a continuation of P.T. Farnsworth's work on IEC fusion devices, R. L. Hirsch was granted a patent [19] on a device containing a spherically or cylindrically symmetrical anode having a concentrically positioned ion-source grid and a cathode that is also spherical or cylindrical and allows the flow of charge through its surface in 1970. It is more complex in its use of additional electrode grids, a thermionic cathode, and the concept of an ion-source grid that is provided with electrons by the thermionic cathode.

The ion-source grid, which is a positively charged wire grid, is used to ionize gas molecules, and is positioned between the anode and cathode in the device. A thermionic cathode is located in the space

between the anode and the grid to produce electrons that oscillate through the openings in the ion-source grid, forming a cloud of electrons around the ion-source grid. The cathode and ion-source grid are both permeable to the flow of the fusion-reacting gas used in the device, including any ions formed during operation of the apparatus. The cathode is hollow, containing no interior supporting structure of any kind. The ion-source grid is at a positive potential in relation to both the anode and cathode. The electric field in the region between the grid and the cathode is of sufficient magnitude to impart fusion reacting energies to particles of positive charge introduced into the second space [that space between the ion-source grid and the cathode].

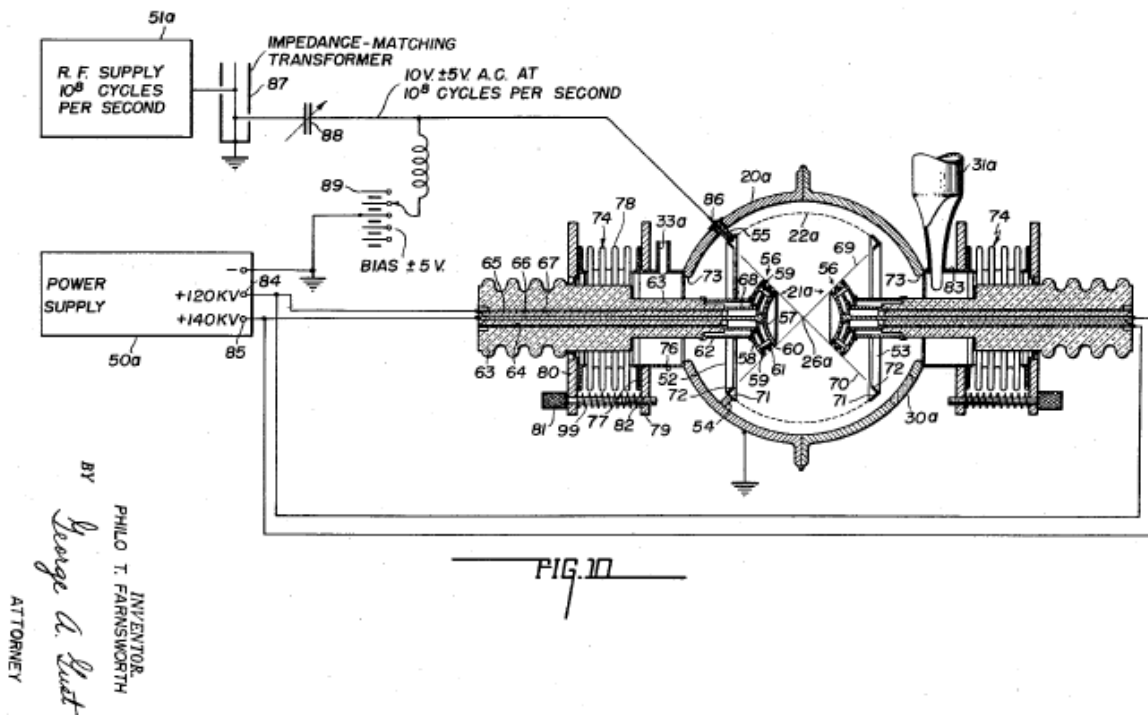


Figure 1.5 Farnsworth's electric discharge device, showing the vacuum chamber and electrical system. Ions are accelerated towards the "virtual cathode" at the center of the device, then oscillate in this space, and interact at nuclear reaction velocities. Figure taken from Ref [19].

In the operation of this invention, the cloud of electrons that has formed primarily from the action of the thermionic cathode surrounds the ion-source grid. This cloud of electrons ionizes neutral gas which

is then accelerated toward the cathode at the center of the device. These ions have a significant probability of interaction with other ions that have been accelerated in this central region. The goal of this apparatus was to create a device that can generate fusion reactions from ions created in spherically symmetric fashion.

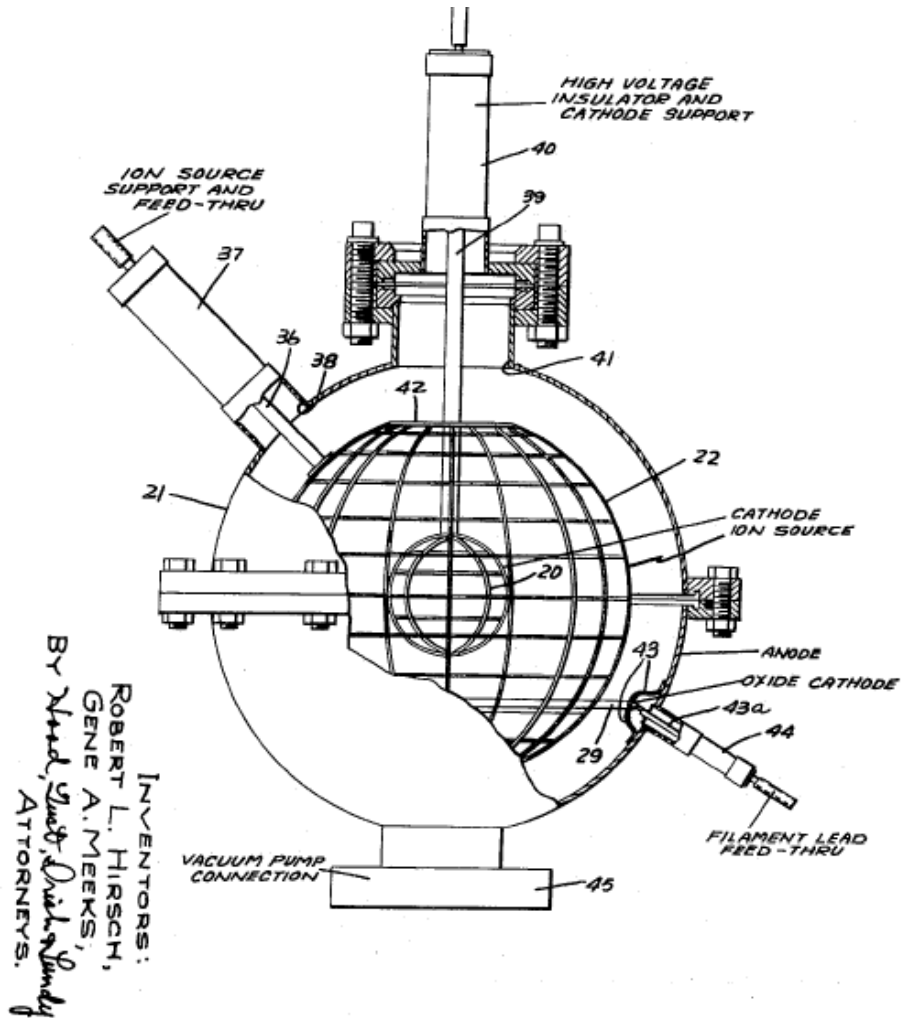


Figure 1.6 Hirsch's apparatus for generating fusion reactions, showing the vacuum chamber and wire grids. In this device, ions are accelerated towards a central point by electric fields. At the central point, interactions between ions with sufficient energy result in nuclear reactions. Figure taken from Ref [20].

1.3 Motivation

Constructing a Farnsworth-Hirsch fusor device at Houghton College will provide a D-D fusion source of neutrons. It is possible to vary the gas pressure in the chamber, the ion source gas composition, the voltage on the inner grid, the vertical position of the outer grounded grid, and the horizontal position of the charged inner sphere. Through changing these variables, the conditions necessary for fusion and neutron production in the Farnsworth Fusor can be examined.

The neutrons produced in D-D fusion reactions in this device could also be used to initiate other nuclear reactions, allowing the Farnsworth fusor to contribute to other nuclear physics experiments. In this device, electron beams emanating from the cathode hit the metal surfaces of the device, producing bremsstrahlung x-rays. These x-rays could also be used in a variety of nuclear physics experiments, such as x-ray fluorescence, x-ray diffraction, biological effects of radiation, and effects of radiation on chemical and physical properties of polymers. The design of this device allows for the measurement of numerous quantities that describe the plasma contained within, including the plasma temperature and emission spectrum. Experiments on the composition of plasma can be completed through varying the ion source gas used and monitoring the measurable quantities of the plasma, such as the plasma temperature, spectrum, and electrical properties through the use of spectrometers and a Langmuir probe. Because of the variety of experiments that can be conducted this device provides the Houghton College physics department with the ability explore a range of topics in nuclear physics.

Chapter 2

THEORY

2.1 Equations of Motion for Plasma

To understand how the particles of the plasma in an inertial electrostatic confinement fusion device move, the equations of motion for a plasma need to be examined. First, a simplified model of the movement of charged particles in \vec{E} and \vec{B} fields is presented, then the equations of motion for plasma, following the development of as presented by J.D. Callen [20] are examined.

2.1.1 Simplest Case: Motion of charged particles in \vec{E} and \vec{B} fields

For a charged particle with charge q in a magnetic field $\vec{B} = B\hat{k}$ and an electric field $\vec{E} = 0$ with velocity $\vec{v} = \vec{v}_\perp + v_\parallel\hat{k}$, the particle moves with the magnetic field providing the centripetal acceleration. The force experienced by the charge due to the magnetic field is given in Equation 2.1, where m is the particle mass, r is the distance of the particle from the origin of the coordinate system, and \vec{v}_\perp is the perpendicular velocity vector.

$$F_c = \frac{-m\vec{v}_\perp^2}{r} = q\vec{v}_\perp \times \vec{B} = -qv_\perp B\hat{r}. \quad 2.1$$

From this, we find the velocity of the particle perpendicular to the magnetic field to be

$$v_\perp = \frac{qBr}{m}. \quad 2.2$$

In Figure 2.1 a diagram of the motion of the charged particle in the magnetic field is shown, where the red dot is the charged particle, r is the distance from the origin to the particle, and the magnetic field \vec{B} is in the z-direction.

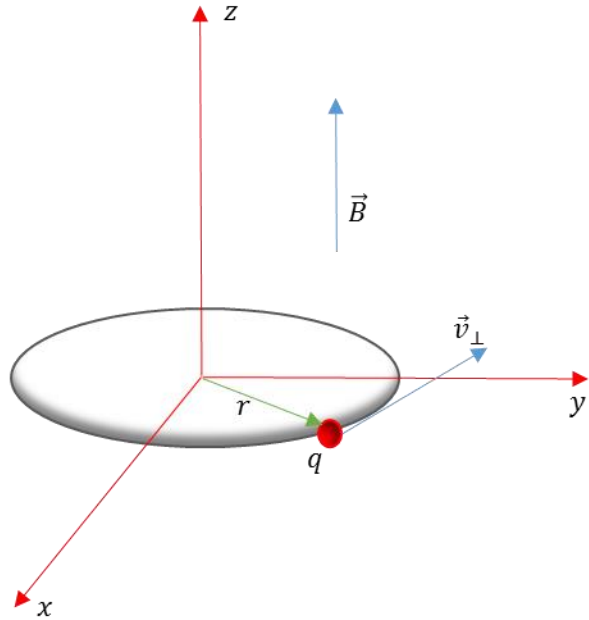


Figure 2.1 A single charged particle in a magnetic field. The red dot is a charged particle, orbiting the origin in a magnetic field \vec{B} .

2.1.2 Exact Kinetic Plasma Equation

In the case of more than one particle, we follow the derivation of the kinetic plasma equations from J.D. Callen [21]. In the development of these equations, the kinetic theory of gases and the hydrodynamics of neutral fluids are considered.

For the many particles in a plasma, we define the charge density, ρ , and current density, \vec{J} , to be

$$\rho = \sum_s n_s q_s, \text{ and} \tag{2.3}$$

$$\vec{J} = \sum_s n_s q_s \vec{v}_s, \tag{2.4}$$

where n_s is the number density of charged particle species s , q_s is the charge of a species s particle, and \vec{V}_s is the flow velocity of species s . In providing a plasma description, we can determine what procedure to use for calculating the charge density, ρ , and the current density \vec{J} , for given electric and magnetic fields \vec{E} and \vec{B} [22]. Because of the complicating factors that cause plasmas to be far from a thermodynamic equilibrium, it is not generally possible to use thermodynamic or statistical mechanics descriptions of plasmas. Therefore, the method proposed by J.D. Callen is a “rigorous *microscopic* description based on the sum of the motions of all the charged particles in a plasma [that] then takes successive averages to obtain kinetic, fluid moment and magnetohydrodynamic (MHD) descriptions of plasmas.

Finding the kinetic description of the motion of charged particles in a plasma begins from an exact microscopic kinetic description that draws from and describes the motions of all the individual charged particles that comprise the plasma. The average properties are found, since the average is more interesting for the purposes of obtaining a general plasma kinetic equation. The particles in a plasma are considered to be point particles; therefore, the spatial distribution of a single particle moving in a trajectory $\vec{x}(t)$ can be represented with the use of the Dirac delta function

$$\delta[\vec{x} - \vec{x}(t)] = \delta[x - x(t)]\delta[y - y(t)]\delta[z - z(t)], \quad 2.5$$

where $\vec{x} = x\hat{i} + y\hat{j} + z\hat{k}$ represents a location in space. In a similar way, the velocities of the particles using the Dirac delta function is

$$\delta[\vec{v} - \vec{v}(t)] = \delta[v_x - v_x(t)]\delta[v_y - v_y(t)]\delta[v_z - v_z(t)]. \quad 2.6$$

If the products of these spatial and velocity-space delta function distributions are added, for each of the $i=1$ to N charged particles of a given species in a plasma is obtained, the “spikey” microscopic distribution f for that species of particles in a plasma,

$$f(\vec{x}, \vec{v}, t) = \sum_{i=1}^N \delta[\vec{x} - \vec{x}_i(t)] \delta[\vec{v} - \vec{v}_i(t)]. \quad 2.7$$

Here N is the number of plasma particles, $\vec{x}_i(t)$ is the position of the i^{th} particle, and $\vec{v}_i(t)$ is the velocity of the i^{th} particle. From this distribution of plasma, we find the particle density by integrating over velocity space,

$$n(\vec{x}, t) \equiv \int_{\text{all velocities}} f(\vec{x}, \vec{v}, t) d^3v = \sum_{i=1}^N \delta[\vec{x} - \vec{x}_i(t)]. \quad 2.8$$

Equation 2.8 is normalized such that its integral over velocity space is the particle number density. If we integrate the number density over all space, the result is N , the number of particles, since

$$\int_{\text{all space}} n(\vec{x}, t) d^3x = \int \sum_{i=1}^N \delta[\vec{x} - \vec{x}_i(t)] d^3x = \sum_{i=1}^N 1 = N. \quad 2.9$$

Through the use of Newton's second law and the Lorentz force, particle trajectories in the "external" \vec{E} and \vec{B} fields can be found. The force on the i^{th} particle is

$$\vec{F}_i = m \frac{d\vec{v}_i}{dt} = q[\vec{E}(\vec{x}_i, t) + \vec{v}_i \times \vec{B}(\vec{x}_i, t)] \quad 2.10$$

where the velocity and position of the i^{th} particle is

$$\vec{v}_i = \frac{d\vec{x}_i}{dt}. \quad 2.11$$

Maxwell's Equations are used to find the fields $\vec{E}(\vec{x}, t)$ and $\vec{B}(\vec{x}, t)$:

$$\vec{\nabla} \cdot \vec{E} = \frac{\rho}{\epsilon_0}, \quad 2.12$$

$$\vec{\nabla} \cdot \vec{B} = 0, \quad 2.13$$

$$\vec{\nabla} \times \vec{E} + \frac{d\vec{B}}{dt} = 0, \text{ and} \quad 2.14$$

$$\vec{\nabla} \times \vec{B} - \frac{1}{c^2} \frac{d\vec{E}}{dt} = \mu_0 \vec{J}. \quad 2.15$$

From Maxwell's Equations it is evident that the charge density, ρ and the current density \vec{J} are the sources of the \vec{E} and \vec{B} fields, which cause the charges to move, which then changes the fields. The charge density ρ and the current density \vec{J} can be found by combining 2.3, 2.4, and 2.8 to get

$$\rho(\vec{x}, t) \equiv \sum_s q_s \int_{\text{all velocities}} f_s(\vec{x}, \vec{v}, t) d^3v = \sum_s q_s \sum_{i=1}^N \delta[\vec{x} - \vec{x}_i(t)], \text{ and} \quad 2.16$$

$$\vec{J}(\vec{x}, t) \equiv \sum_s q_s \int \vec{v} f_s(\vec{x}, \vec{v}, t) d^3v = \sum_s q_s \sum_{i=1}^N \vec{v}_i(t) \delta[\vec{x} - \vec{x}_i(t)]. \quad 2.17$$

Equations 2.10 through 2.17, along with the initial conditions for all N of the particles give a description of the exact motion of all the charged particles of a plasma, and charge and current densities, the \vec{E} and \vec{B} fields that the particles create, and the effect these fields have on the motion of the plasma particles. In this way, a “complete and exact microscopic description of a plasma” is created [23]. Unfortunately, for a macroscopic plasma of 10^{16} to 10^{24} particles, using this method is extremely difficult because it requires the use of a very large number of equations. In addition, the quantity of information provided through this method is far beyond what is needed in practical applications. Therefore, an average can be used to find a numerical solution for $\vec{x}(t)$ and $\vec{v}(t)$ for all N particles.

2.1.3 Numerical Approximation for Kinetic Plasma Equations

To simplify the equations of motion, we determine how the particle distribution function f changes with time.

$$\frac{df(\vec{x}, \vec{v}, t)}{dt} = \frac{\partial f}{\partial t} + \sum_{j=1}^3 \frac{\partial f}{\partial x_j} \frac{\partial x_j}{\partial t} + \sum_{j=1}^3 \frac{\partial f}{\partial v_j} \frac{\partial v_j}{\partial t}, \quad 2.18$$

where x_j and v_j are the components of the position and velocity of the distribution function f . This can be rewritten to incorporate the Dirac delta form of f given in Equation 2.7

$$\frac{df(\vec{x}, \vec{v}, t)}{dt} = \left[\frac{\partial}{\partial t} + \sum_{j=1}^3 \frac{\partial x_j}{\partial t} \frac{\partial}{\partial x_j} + \sum_{j=1}^3 \frac{\partial v_j}{\partial t} \frac{\partial}{\partial v_j} \right] \sum_{i=1}^N \delta[\vec{x} - \vec{x}_i(t)] \delta[\vec{v} - \vec{v}_i(t)]. \quad 2.19$$

From the properties of the Dirac delta, further simplification of the equation of the time derivative of f is possible. The time derivative of the Dirac delta functions can be used;

$$\frac{\partial}{\partial t} \delta[\vec{x} - \vec{x}_i(t)] = \sum_{j=1}^3 \frac{dx_{ij}}{dt} \frac{\partial}{\partial x_j} \delta[\vec{x} - \vec{x}_i(t)], \text{ and} \quad 2.20$$

$$\frac{\partial}{\partial t} \delta[\vec{v} - \vec{v}_i(t)] = \sum_{j=1}^3 \frac{dv_{ij}}{dt} \frac{\partial}{\partial v_j} \delta[\vec{v} - \vec{v}_i(t)]. \quad 2.21$$

In these equations, x_{ij} and v_{ij} are the j^{th} components of position and velocity for the i^{th} particle. Using these, Equation 2.19 maybe be simplified.

$$\frac{df}{dt} = \sum_{i=1}^N \left\{ - \sum_{j=1}^3 \frac{dx_{ij}}{dt} \frac{\partial}{\partial x_j} \delta[\vec{x} - \vec{x}_i(t)] \delta[\vec{v} - \vec{v}_i(t)] - \sum_{j=1}^3 \frac{dv_{ij}}{dt} \frac{\partial}{\partial v_j} \delta[\vec{x} - \vec{x}_i(t)] \delta[\vec{v} - \vec{v}_i(t)] \right. \\ \left. + \sum_{j=1}^3 \frac{dx_j}{dt} \frac{\partial}{\partial x_j} \delta[\vec{x} - \vec{x}_i(t)] \delta[\vec{v} - \vec{v}_i(t)] + \sum_{j=1}^3 \frac{dv_j}{dt} \frac{\partial}{\partial v_j} \delta[\vec{x} - \vec{x}_i(t)] \delta[\vec{v} - \vec{v}_i(t)] \right\},$$

2.22

which reduces to

$$\frac{df}{dt} = \sum_{i=1}^N \sum_{j=1}^3 \left\{ - \frac{dx_{ij}}{dt} \frac{\partial}{\partial x_j} + \frac{dx_j}{dt} \frac{\partial}{\partial x_j} - \frac{dv_{ij}}{dt} \frac{\partial}{\partial v_j} + \frac{dv_j}{dt} \frac{\partial}{\partial v_j} \right\} \delta[\vec{x} - \vec{x}_i(t)] \delta[\vec{v} - \vec{v}_i(t)]. \quad 2.23$$

Now, the delta are only non-zero only when $\vec{x} = \vec{x}_i$ and $\vec{v} = \vec{v}_i$, but when this is the case, the derivative terms cancel. Therefore

$$\frac{df}{dt} = 0. \quad 2.24$$

Going back to Equation 2.18

$$\frac{df}{dt} = \frac{\partial f}{\partial t} + \sum_{j=1}^3 \frac{\partial f}{\partial x_j} \frac{dx_j}{dt} + \sum_{j=1}^3 \frac{\partial f}{\partial v_j} \frac{dv_j}{dt} = 0. \quad 2.25$$

We see that this can be written in terms of the gradients

$$\frac{df}{dt} = \frac{\partial f}{\partial t} + \vec{v} \cdot \vec{\nabla}_x f + \frac{d\vec{v}}{dt} \cdot \vec{\nabla}_v f. \quad 2.26$$

With further manipulation, a simplified form that describes the microscopic plasma system can be found

$$\frac{df}{dt} = \left\{ \frac{\partial}{\partial t} + \vec{v} \cdot \vec{\nabla}_x + \frac{d\vec{v}}{dt} \cdot \vec{\nabla}_v \right\} \sum_{i=1}^N \delta[\vec{x} - \vec{x}_i(t)] \delta[\vec{v} - \vec{v}_i(t)]. \quad 2.27$$

The operator term is moved inside the summation:

$$\frac{df}{dt} = \sum_{i=1}^N \left\{ \frac{\partial}{\partial t} + \vec{v}_i \cdot \vec{\nabla}_x + \frac{d\vec{v}_i}{dt} \cdot \vec{\nabla}_v \right\} \delta[\vec{x} - \vec{x}_i(t)] \delta[\vec{v} - \vec{v}_i(t)]. \quad 2.28$$

Since $\vec{F}_i = m \frac{d\vec{v}_i}{dt}$, Equation 2.10 is inserted for \vec{F}_i :

$$\frac{df}{dt} = \sum_{i=1}^N \left\{ \frac{\partial}{\partial t} + \vec{v}_i \cdot \vec{\nabla}_x + \frac{q}{m} [\vec{E}(\vec{x}_i, t) + \vec{v}_i \times \vec{B}(\vec{x}_i, t)] \cdot \vec{\nabla}_v \right\} \delta[\vec{x} - \vec{x}_i(t)] \delta[\vec{v} - \vec{v}_i(t)]. \quad 2.29$$

Since the Dirac delta is non-zero only where $\vec{x} = \vec{x}_i$ and $\vec{v} = \vec{v}_i$, Equation 2.29 can be simplified to what is called the Klimontovich equation:

$$\frac{df}{dt} = \left\{ \frac{\partial}{\partial t} + \vec{v} \cdot \vec{\nabla}_x + \frac{q}{m} [\vec{E}(\vec{x}, t) + \vec{v} \times \vec{B}(\vec{x}, t)] \cdot \vec{\nabla}_v \right\} f = 0. \quad 2.30$$

Equation 2.30 provides a complete, exact description of the microscopic plasma system that is equivalent to that in 2.8-2.18.

2.1.4 *Averaging the Klimontovich Equation*

To obtain the kinetic plasma description, the Klimontovich equation, Equation 2.30, is averaged using the simple, more physical procedure described by Callen. First, the number of particles N_{6D} in a small box in a six-dimensional phase space of spatial volume $\Delta V \equiv \Delta x \Delta y \Delta z$, and velocity-space volume $\Delta V_v \equiv \Delta v_x \Delta v_y \Delta v_z$ is $N_{6D} \equiv \int_{\Delta V} d^3x \int_{\Delta V_v} d^3v f$. The box is defined so that the box size is large

compared to the average spacing of particles in the plasma, so that any statistical fluctuations in the number of particles in the box will be small [24]. On the other hand, the box should not be too large, or the macroscopic properties of the plasma may vary significantly within the volume of the box. This will be the case if we average the Klimontovich equation over a scale $n^{-\frac{1}{3}} < \Delta x < \lambda_D$ and $\left(\frac{V_t}{n\lambda_D^3}\right)^{\frac{1}{3}} < \Delta V$, where λ_D is the Debye length.

The average of the distribution in Equation 2.30 can now be taken, where $C(f)$ accounts for coulomb collisions in the plasma,

$$\frac{d\langle f \rangle}{dt} = \left\{ \frac{\partial}{\partial t} + \vec{v} \cdot \vec{\nabla}_x + \frac{q}{m} [\vec{E}(\vec{x}, t) + \vec{v} \times \vec{B}(\vec{x}, t)] \cdot \vec{\nabla}_v \right\} \langle f \rangle = C(f). \quad 2.31$$

In the case of the low pressure plasma, when $C(f) = 0$,

$$\frac{d\langle f \rangle}{dt} = \left\{ \frac{\partial}{\partial t} + \vec{v} \cdot \vec{\nabla}_x + \frac{q}{m} [\vec{E}(\vec{x}, t) + \vec{v} \times \vec{B}(\vec{x}, t)] \cdot \vec{\nabla}_v \right\} \langle f \rangle = 0. \quad 2.32$$

This is called the Vlasov equation, which is the kinetic equation that describes collisionless plasma on short time scales. Now, it is possible to find $\langle f \rangle$ by utilizing the Vlasov equation. Using the distribution function $\langle f \rangle$, the charge and current distributions are found

$$\rho(\vec{x}, t) \equiv \sum_s q_s \langle f_s \rangle d^3 v, \text{ and} \quad 2.33$$

$$\vec{J}(\vec{x}, t) \equiv \sum_s q_s \vec{v} \langle f_s \rangle d^3 v. \quad 2.34$$

From these equations, \vec{E} and \vec{B} can be calculated with the use of Maxwell's equations. It must be noted that this process of calculation has not "closed the loop", since these fields also determine the distribution function $\langle f \rangle$.

2.2 Lawson's Criterion for Fusion

In an effort to understand what conditions are necessary to construct and operate a controlled thermonuclear reactor capable of producing a useful quantity of power, John D. Lawson investigated the conditions that exist in two varieties of reactors [10]. In this way, a set of criteria describing the operation of usefully productive thermonuclear reactors was developed.

2.2.1 *Premise of Criteria*

For a thermonuclear reactor, the exoergic reactions between the hydrogen isotopes are the most promising for energy production at low energies. The tritium-deuterium (T-D) reaction has a larger cross section and releases more energy than other reactions, but the production of tritium makes it more costly than the naturally occurring hydrogen isotope deuterium.

The energy released per unit time and volume in a thermonuclear reaction in a hot gas is given by $P_R = n_1 n_2 \bar{v}\sigma(T)E$ [25], in which n_1 and n_2 are the number densities of the two kinds of nuclei, and the term $\bar{v}\sigma(T)$ is determined from experimentally derived values for the D-D and T-D cross sections. The power P_R is proportional to the number of particles n_1 and n_2 , as well as the energy E of a reaction. The proportionality constant, $\bar{v}\sigma(T)$ is the average of the reaction cross section at a given temperature multiplied by the particle velocities at this temperature.

Knowing this, it is possible to analyze where energy is lost from the hot gas. Energy from the hot gas can be lost by processes of radiation and conduction. At temperatures around 10^6 °C in a reactor, hydrogen is completely ionized, and therefore the majority of radiation emitted is bremsstrahlung. There are no other normal mechanisms for the release of energy through radiation in this situation. This is because the mean free path of this bremsstrahlung radiation is quite large, on the order of several g/cm². Another source of energy loss in a thermonuclear reactor system due to radiation emission could be the radiation produced by the acceleration of electrons in magnetic fields within the system. It is possible to ignore this effect, however, because the magnetic fields within the system are not intense enough to produce a significant energy loss.

Energy loss through conduction is challenging to quantify, since it is entirely dependent on the construction of the thermonuclear reactor system. It is necessary to know the geometry of the system, the density and temperature distribution of the hot gases within the system, and the physical properties of the materials that used in the construction of the walls. Because of the challenge of determining this energy loss, it is much easier to assume that the loss of energy due to conduction is zero. This assumption is reasonable, since for this type of reaction system the reaction occurs in a region surrounded by a vacuum.

2.2.2 *Systems in Which the Reaction Products are Retained*

In systems where the charged reaction products in the hot gas are retained by the electric and magnetic fields of the system, such as in IEC fusion or magnetic confinement fusion, Equation 2.35 can be used to find the temperatures at which a system is self-sustaining in the absence of loss of energy due to conduction. For the D-D reaction the temperature was found to be about 3×10^8 degrees, and for the T-D reaction it is 5×10^7 degrees. It is important to note that in this design of a thermonuclear reactor system, the D-D fusion reaction is only sustainable for a very narrow temperature range, because at temperatures greater than that required for a self-sustaining reaction, energy loss due to radiation causes the self-sustaining nature of the reaction to cease.

Chapter 3

EXPERIMENT & APPARATUS

3.1 Experimental overview

In this chapter, the construction details of the Farnsworth-type fusor that was built at Houghton College are discussed. The vacuum system, high voltage electrical system, measurement devices, radiation detection, and radiation safety devices are covered.

3.2 Vacuum System

3.2.1 *Vacuum pumps and cold trap*

For proper operation of the Farnsworth fusor, initial pressures in the range of 10^{-6} Torr are required. First, an Alcatel model ZM2008A rotary forepump is used to reduce the pressure in the vacuum chamber to 10^{-3} Torr. The forepump functions through the rotation of an off-center rotor within the cylindrical pump stator, which draws in gas through the intake, compresses this gas, then vents the gas through the exhaust valve. This vacuum pump is connected via rubber vacuum hose to a Varian model 0159 diffusion pump, which allows the chamber to be evacuated to the range of 10^{-6} Torr. The diffusion pump functions by heating an oil to a vapor which is directed to spray down toward the gas outlet to the forepump. A Kurt J. Lesker company model #TLR6XS150QF cold trap is mounted directly above the diffusion pump, and if filled with liquid nitrogen at 77 K, contributes to the evacuation of the chamber to pressures of nearly 10^{-7} Torr by slowing gas molecules and trapping water molecules with the oil vapor spray.

3.2.2 *Vacuum chamber*

The main vacuum chamber of the Farnsworth Fusor is a stainless steel 0.35 m diameter bell jar with 18 ports of several sizes of conflat flanges (CF). There are four 8 CF ports located equatorially, with four 2.75 CF ports interspersed between the 8 CF ports. On the upper curved surface of the chamber, there are two 4 CF ports and six 2.75 CF ports. At the top of the device, there is a 6 CF port. The lower 0.35 m opening of the bell-jar vacuum chamber is connected to reducer that leads to an 8 CF port. The ports, with the exception of the lower 0.35 m CF port, have been numbered one through seventeen. The ports

on the vacuum chamber are numbered in Table 3-1. In Figure 3.2, a photograph of the Farnsworth fusor in the laboratory gives a view of the diffusion pump, cold trap, and the main vacuum chamber with the attachments described in Table 3-1.

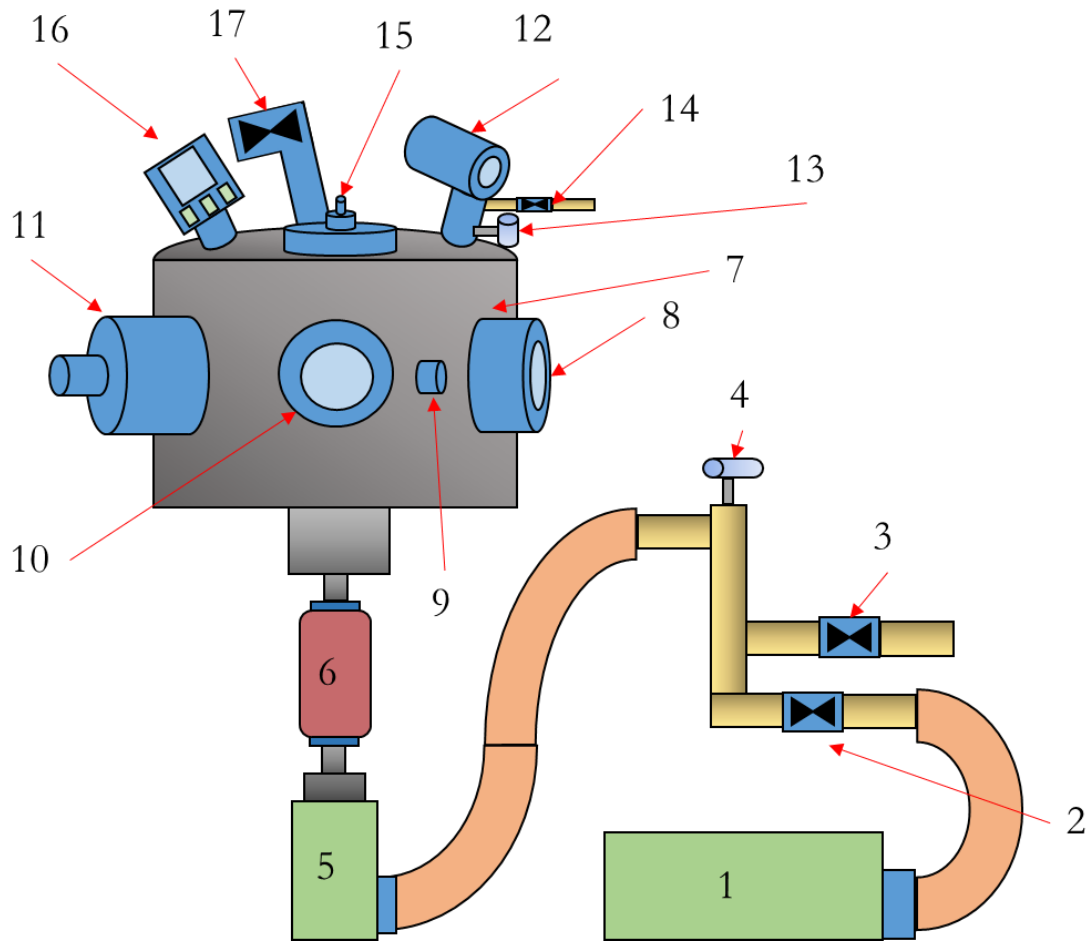


Figure 3.1 In the vacuum system, the forepump (1) provides evacuation down to between 10^{-2} and 10^{-3} Torr. Valve (2) allows the forepump to pump from the chamber. The up-to-air valve (3) allows air to enter the vacuum system. A pirani gauge (4) measures the air pressure in the foreline. Pressures down to 10^{-6} Torr are obtained using the diffusion pump (5) and the cold trap (6). Ports on the vacuum chamber (7) are labeled: port 5 (8), port 6 (9), port 7 (10), and port 8 (11). A hot cathode ion gauge (12) and a pirani gauge (13) monitor the chamber pressure. The up-to-air valve (14) is attached at this site as well. Port 17 (15) contains the electrical feedthrough and linear motion feedthrough for the outer electrode grid. A CCM501 cold cathode ion gauge (16) is mounted on port 15. A variable leak valve is attached to an angle valve on port 16 (17).

Table 3-1 The assignment of ports on the Farnsworth fusor vacuum chamber.

Port #	Note
1	2.75 CF adapted to 1.33 CF for HV feedthrough for interior electrode grid
2	linear motion feedthrough 2.75 CF for interior electrode grid
3	blank 8 CF
4	blank 2.75 CF
5	8 CF viewport with 8 CF blank steel shield covering the glass aperture
6	2.75 CF blank
7	8 CF viewport with 8 steel shield covering the glass aperture
8	8 CF port adapted to 2.75 CF adapted to 1.33 CF port with 6.35 mm diameter metallized BoPET window 0.0122 mm thick
9	2.75 CF port adapted to KF 16
10	4 CF blank
11	2.75 CF blank
12	2.75 CF port with I-100-K ion gauge, Whitey up to air valve, and Granville convectron gauge
13	2.75 CF blank
14	4 CF blank
15	2.75 CF with 90 deg elbow to cold cathode ion gauge model InstruTech CCM501FD
16	2.75 CF with Varian Model 951-5013 angle valve to Varian variable leak valve model 951-5100
17	6 CF port adapted to 2.75 CF with linear motion feedthrough for the grounded electrode, and the ground electrode output.
18	14 CF connected to vacuum system through cold trap.

3.2.3 *Vacuum leak valve*

As mentioned in Section 3.2.2, on port 16 a Varian model 951-5100 variable leak valve is attached to a Varian Model 951-5013 angle valve. The leak valve allows gas into the fusor chamber, at a minimum leak rate of 1×10^{-9} Torr-liters/second through an optically flat sapphire crystal and a copper metal gasket aperture. The angle valve closes the chamber from the leak valve when no leak is desired. The up-to-air pressure valve on port 12 brings the chamber up to atmospheric pressure after the diffusion pump has been shut off.

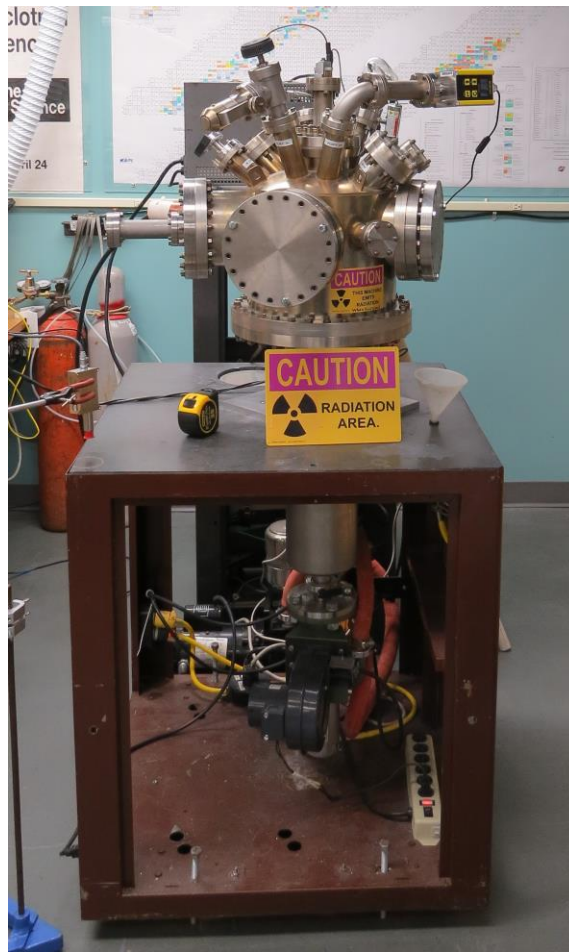


Figure 3.2 The Houghton College Farnsworth-Hirsch fusor. The diffusion pump and cold trap are below the table surface, and the cold-cathode ion gauge is mounted on the top right of the device.

3.2.4 Gas Pressure

There are four gas pressure sensors attached to the fusor, as seen in Figure 3.1. The two pirani type Granville-Phillips Convectron gauges measure down to the millitorr range. The pirani gauge mounted between the forepump and the diffusion pump measures the foreline pressure. A Duniway Stockroom Corp. I-100-K hot cathode ion gauge can measure pressures from 1×10^{-3} Torr to 2×10^{-10} Torr, and is attached at port 12 on the vacuum chamber. The pirani gauges and the I-100-K hot cathode ion gauge are both read with a Stanford Research Systems IGC100 ion gauge controller. During the operation of the fusor, it is necessary to disconnect the hot cathode ion gauge and the pirani gauges to avoid the possibility of damage being done to these sensitive electronic devices by the high voltage electricity. An InstruTech, Inc. Series 501 Hornet™ Cold Cathode Miniature Ionization Vacuum Gauge (CCM501FD) that operates in the range of 1×10^{-2} to 1×10^{-8} Torr was also used to determine the pressure in the fusor chamber during the operation of the high voltage system. The cold cathode ion gauge is more rugged and has a reduced risk of being damaged by the high voltages used in the fusor. In addition, a metal mesh was placed in the 90 degree elbow on port 15 before the cold cathode ion gauge to further protect the gauge.

During the testing of the pressure gauges, it was found that the I-100-K hot cathode ion gauge and the CCM501FD cold cathode ion gauge were calibrated differently. The pressure measurements from these gauges, when plotted in Figure 3.3, are linear, but are calibrated differently.

3.3 High Voltage System

3.3.1 Wire Grids

For the construction of the electrical system of the fusor, two wire grids, each composed of 0.63 mm (0.025 inch) diameter 304 stainless steel wire were constructed using a Sunstone Engineering CD160 DPM2 capacitive discharge spot welder. It was found that for each type of weld, a distinct weld energy was required. The energies required for welds used in the construction of the grids are listed in Table 3-2. If the weld energy was incorrect, the wires either did not weld, or exploded. Conflat flanges of 2.75, 6, and 8 inches in diameter were used as forms to shape circular wire rings that were welded together to form the spherical grids used in the fusor.

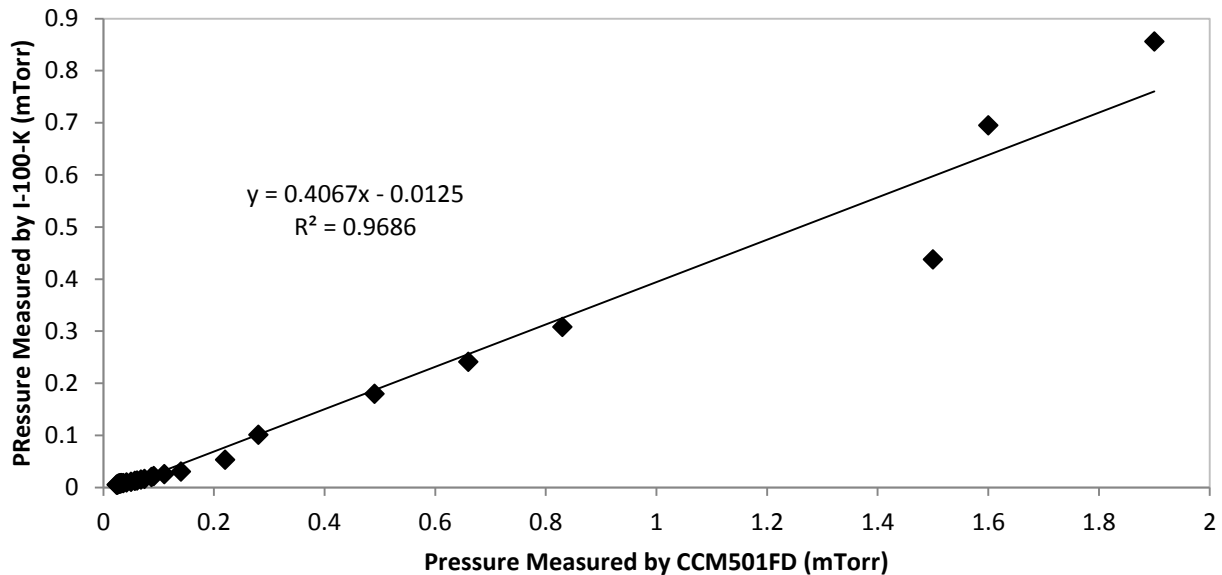


Figure 3.3 A plot generated by a comparison of the pressure data collected simultaneously from the I-100-K hot cathode ion gauge and the CCM501FD cold cathode ion gauge in the operating pressure range of the fusor. The linear trend observed in these data, does not have a slope of one, so the two gauges are calibrated differently.

For the larger 20.3 cm diameter grid, two 20.3 cm rings that had been formed with the 8 CF flange were welded together at a 90° angle to form the basic sphere form. Next, two 15.2 cm diameter rings were welded at the 60° latitude lines. The junction on one pole of the 20.3 cm wire grid was spot-welded to a 3.8 cm long section of an M4 threaded steel rod. The section of M4 threaded rod is screwed to a piece of ceramic insulator, which is screwed to the linear motion feedthrough on port 17. In Figure 3.3, this grid is the outer grid connected to earth ground.

The smaller, 7.0 cm grid was constructed from three wire rings made using a 2.75 conflat flange as a template. For this spherical grid, two of these rings were welded together at a 90°. Then, the third 7.0 cm ring was attached on the equator with one weld at each of the four wire junctions. Once completed, the small wire sphere was welded to a section of Du-Bro 173 2-56 steel threaded rod. The threaded rod was screwed into a piece of ceramic insulator that connects to the end of the linear motion feedthrough

on port 2. In Figure 3.4, this grid is the inner grid connected to the negative terminal of the high voltage power supply through a ballast resistor.

Table 3-2 The empirically best capacitive discharge weld energy for constructing the wire grids. Pulse 1 cleans the weld site. Pulse 2 causes welds. The abbreviations are: WSbS—wires side by side; WEtE—wires end to end; WL 90°—wires layered at 90°.

Weld Type	Pulse 1 % Energy	Pulse 2 % Energy	Weld Energy (ws)	Weld Strength
WSbS	10	90	100	strong
WEtE	10	90	150	thin
WEtE	10	90	120	thin
WEtE	10	90	120	moderate
WEtE	10	90	110	thin
WEtE	10	90	100	no weld
WL 90°	10	90	120	no weld
WL 90°	10	90	100	thin
WL 90°	10	90	80	strong
WL 90°	10	90	75	strong
WL 90°	10	90	50	strong

3.3.2 High Voltage Power Supply and Ballast Resistor

A Sorensen 230-3/12P R&D high voltage power supply, providing up to 3 mA at 30 kV, was used to provide the negative potential on the inner wire grid. The inner wire grid is connected through the electrical feedthrough on port 1 of the vacuum chamber through a 1.5 M Ω 7-watt resistor. This ballast resistor functions by decreasing the voltage across the electrodes, so that during high current flows, for example, when a spark occurs, the voltage drops, causing a drop in current. The power supply features a circuit breaker that shuts off above 3 mA while operating in the 30 kV mode.

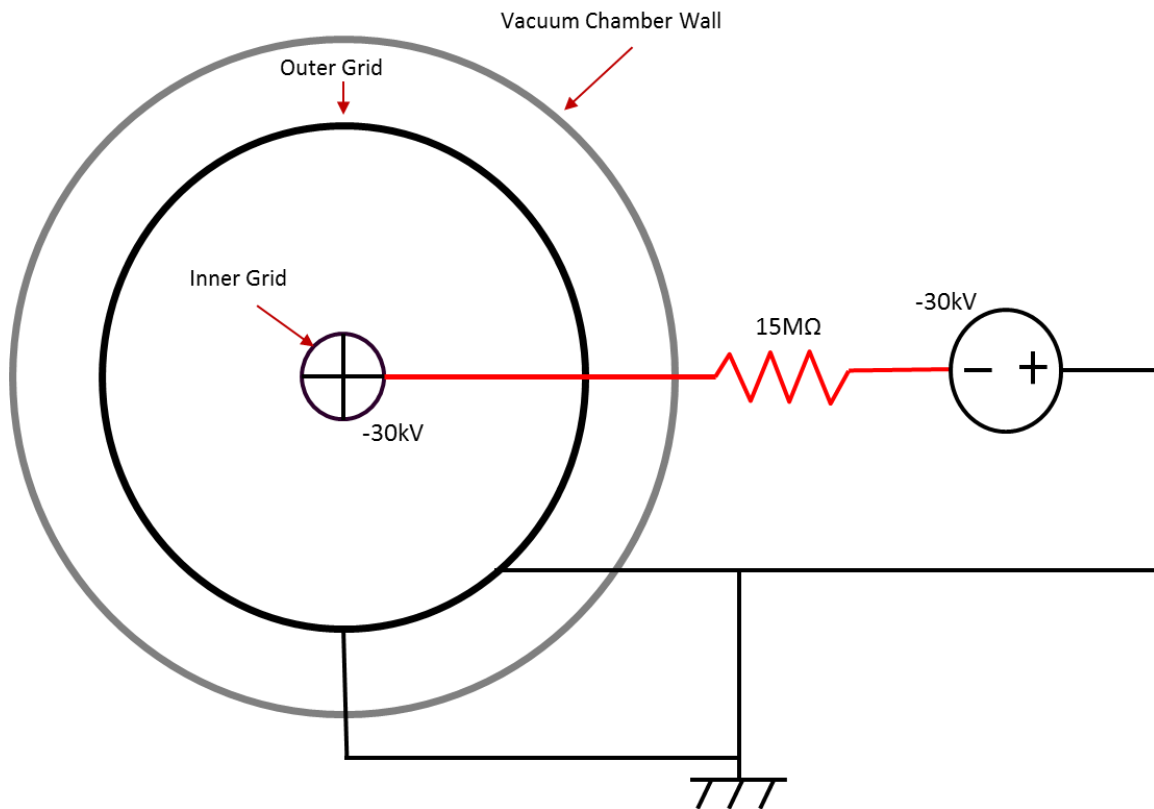


Figure 3.4 A schematic diagram of the Farnsworth-type fusor. A high voltage power supply provides a potential of up to -30kV to the inner electrode grid. The outer grid and the walls of the vacuum chamber are grounded.

3.3.3 Safety Shield

A grounded electrical safety shield surrounds the end of the high voltage line, ballast resistor, and electrical feedthrough to the vacuum chamber. It is made from a 21 cm long section of PVC pipe with an interior diameter of 4.0 cm and exterior diameter of 4.9 cm that surrounded by a 15 cm long copper pipe which is grounded through its connection to the chamber by the aluminum strips holding it in place on the vacuum chamber port. The copper pipe has an interior diameter of 5 cm and an exterior diameter of 5.4 cm. The grounded safety protects the operators, but for the highest voltages, sparking from the high voltage line to the copper shield sometimes occurs.

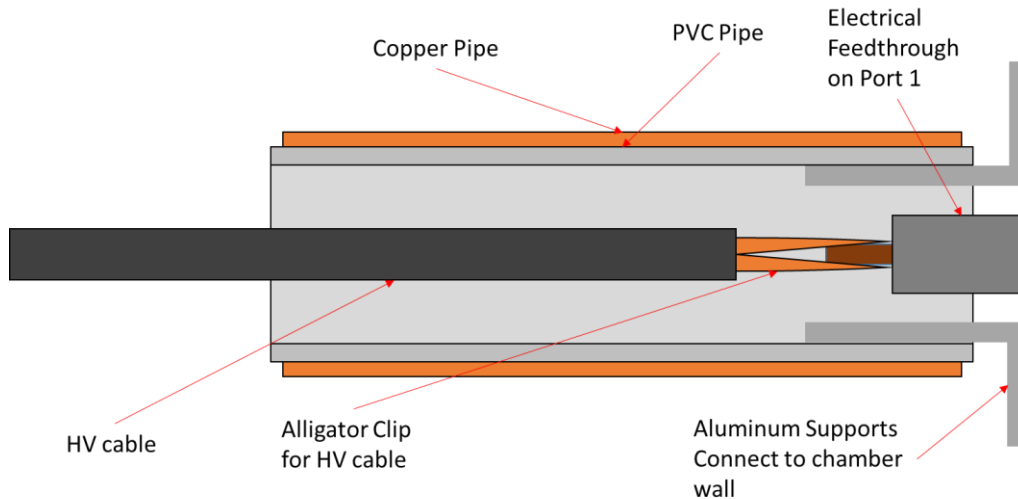


Figure 3.5 The high voltage safety shield is grounded through its connection to the Farnsworth fusor chamber. It covers the end of the high voltage line where a connection is made with the electrical feedthrough. It is composed of concentric PVC and copper tubes.

3.3.4 *Voltage and Current*

The voltage and current supplied to the Farnsworth fusor circuit are measured using the voltmeter and ammeter in the Sorensen 230-3/12P R&D high voltage power supply.

3.3.5 *Electrode Positioning*

The two electrodes within the chamber can be moved with their associated linear motion feedthroughs. Port 2 contains a linear motion feedthrough that controls the horizontal linear motion of the charged inner electrode and is set to have the small grid positioned at the center. Port 17 contains the linear motion feedthrough for the vertical position of the grounded outer electrode, which is set to have the inner electrode centered inside the outer grid.

3.4 **Radiation Measurements**

3.4.1 *X-Ray Measurements*

An Amptek XR-100T CdTe γ /x-ray detector with its accompanying PX2T-CZT power supply and amplifier was used to collect x-ray spectra from the Farnsworth fusor from several ports and distances.

The spectra were recorded with an Amptek MCA8000A “Pocket MCA”. A multimeter was used to monitor the temperature of the x-ray sensor. A calibrated Ludlum Measurements, Inc. Model 3 survey meter was used to monitor radiation dose rates.

3.5 **Radiation Safety**

Proper radiation safety measures were followed when conducting these experiments. Houghton College has a comprehensive radiation safety training course that is in accordance with NYDOH guidelines. All student researchers working with radiation machines are required to complete this course and pass the post-test prior to starting work.

3.5.1 *Application of ALARA*

As a part of the implementation of proper radiation safety at Houghton College, the principle of ALARA, or As Low As Reasonably Achievable, is followed. In experiments at Houghton, student researchers and faculty are required to, if possible: 1. Minimize time in a field of radiation; 2. Maximize distance from a source of radiation; 3. Use shielding whenever practicable; 4. Use source reduction whenever possible.

3.5.2 *Implementation of ALARA for this project*

In these initial tests of the Houghton College Farnsworth fusor, the principle of ALARA was taken into account. To minimize time spent in a radiation field, the device was turned off as soon as it was no longer needed. During the operation of the device, the operator was located several feet away, and other personnel were kept at distances further away. All viewports of the device were covered with steel shielding plates when not in use. The hot cathode ion gauge on port 12, which is pointed upward, is composed of thin glass, and will be removed to further reduce emission of x-ray radiation. Port 8, the Mylar BoPET window, is protected by a length of steel CF tubing that collimates the x-ray radiation. The outer aperture of this collimator is normally covered by a 2.75 CF flange. An area monitor in the room alarms if the radiation dose rate is measured above a safe level.

Measurements of the radiation from the fusor range from background of less than 0.1 mR/hr at the steel viewport shields to around 400 mR/hr at the aperture of the collimator of the Mylar BoPET window. Further discussion of the radiation measurements is found in Section 4.2.

3.5.3 *Future Implementation of ALARA for this project*

For the future operation of the Farnsworth fusor, it is planned that all systems of device will be operated remotely. For the control of the high voltage, a remotely controlled Bertan Series 815 power supply will be able to continuously monitor the output voltage and current. To monitor the pressure inside the vacuum chamber remotely, the CCM501FD gauge can be interfaced with a computer through an RS-485 connection. An APEX Series 16 computerized mass flow controller will control the chamber pressure from the remote location. The door to the room containing the Farnsworth fusor has an interlock system that can be enabled to prevent the operation of the fusor when the doors are open.

Chapter 4

RESULTS & ANALYSIS

4.1 Voltage/Current/Pressure Measurement

A series of tests were conducted using the Farnsworth fusor, and the pressure, current, and voltage were recorded. The pressure in the chamber was set, then the high voltage power supply was turned on, and the voltage was increased incrementally. As the voltage was increased, the current was recorded as soon as the current reading on the power supply current monitor stabilized. It can be observed from Figure 4.1 that as the potential was increased, the current increased accordingly. If the potential increased beyond 30 kV, sparking occurred. At currents above 3 mA, the high voltage power supply overload trips off. For voltages less than 22 kV at the pressures selected, a plasma did not form. Therefore, a current was not observed in the circuit until a plasma formed above voltages of 22 kV.

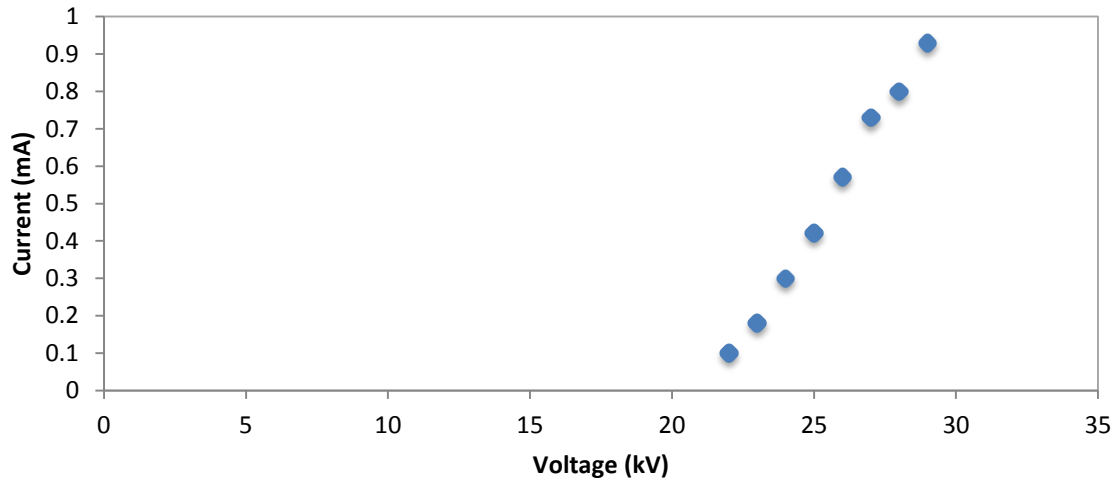


Figure 4.1 A plot of the power supply current as a function of voltage at a set pressure in the vacuum chamber at 2.94×10^{-4} Torr. For voltages less than 22 kV, a plasma did not form. For this data, the current abruptly jumped to overload past 1 mA.

4.2 Radiation Measurement

4.2.1 Dose Rates

The dose rate was measured with the Ludlum Measurements, Inc. Model 3 survey meter at several distances away from the device. The operating parameters are in Table 4-1. The survey meter was held at distances of 0.00, 0.51, 0.76, 1.02, 1.78, and 2.36 m away from port 8, the thin Mylar window, as measured with a measuring tape. The results are in Figure 4.2.

Table 4-1 The operating parameters of the fusor for the dose rate measurements.

Voltage (KV)	26
Current (mA)	2
Pressure (mtorr)	0.8
Resistor (M Ω)	1

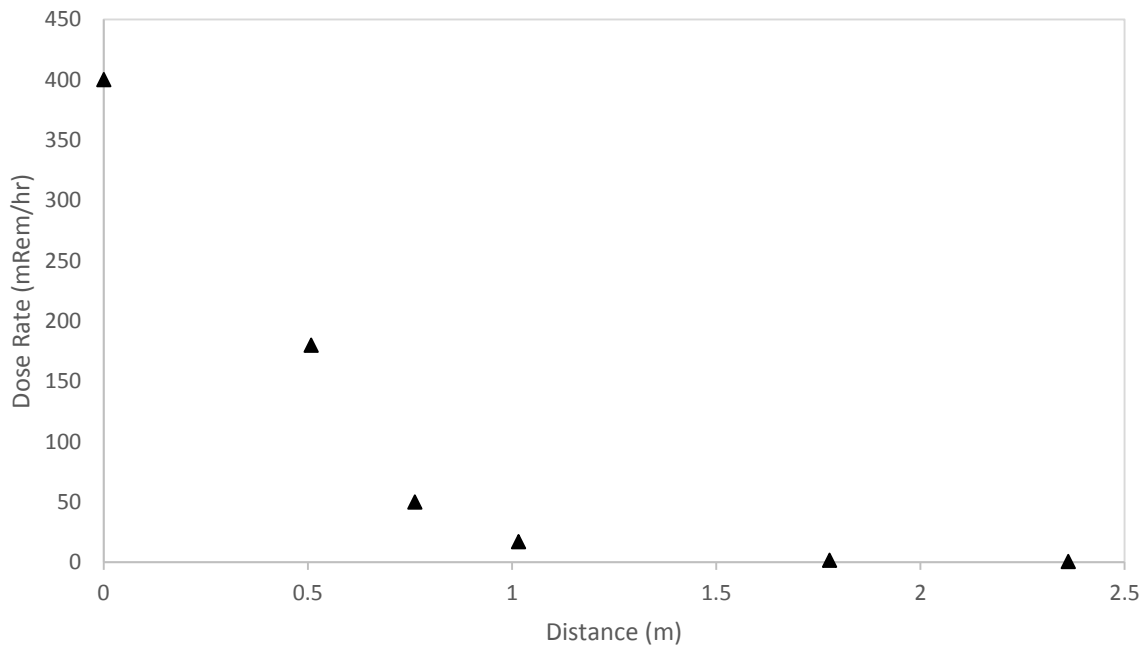


Figure 4.2 X-ray dose rate as a function of distance from the collimator aperture of port 8.

To determine the approximate angular dependence of the x-ray beam, dose rate measurements, with the fusor at the same operating parameters in Table 4-1, were collected at points along a line perpendicular to the 1.78 m line, as in Figure 4.3. The dose rate was measured at increments of 2.5 cm to the left and right of the center point, until it reached background. The dose rates are plotted in Figure 4.4.

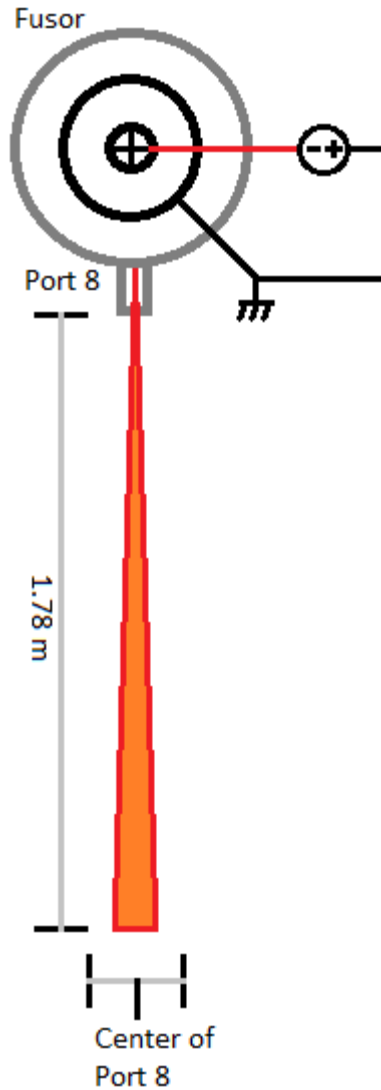


Figure 4.3 To measure the angular dependence of the dose rate at a distance of 1.78 m from port 8, the survey meter was moved along a line perpendicular to the 1.78 m distance from port 8.

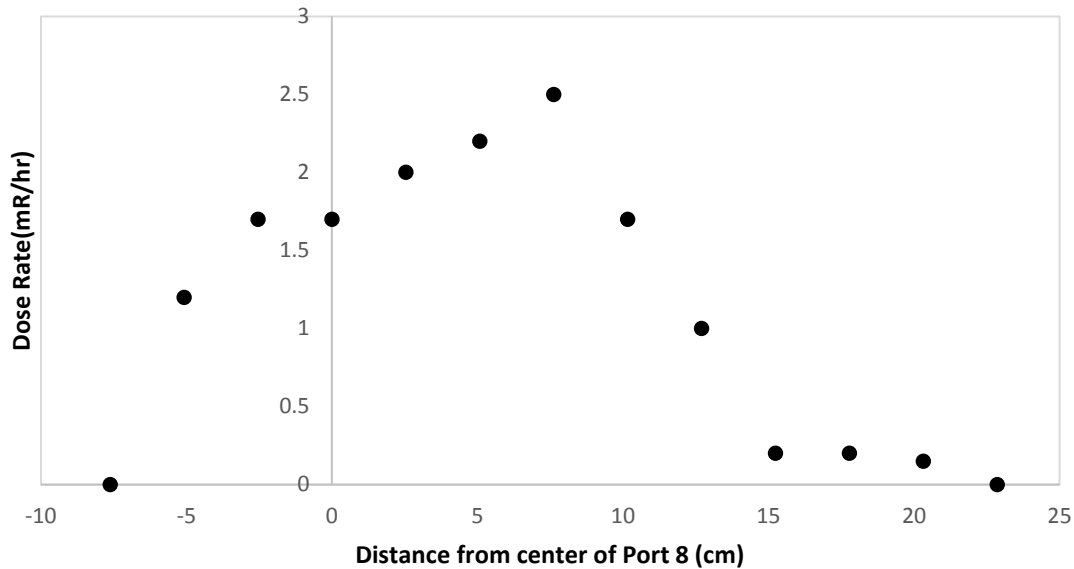


Figure 4.4 A plot of the data collected in the horizontal dose rate distribution test at 1.778 m from the aperture of port 8. The approximate diameter of the radiation cone at 1.778 m was found to be 23 cm.

4.2.2 X-ray Spectra

The Amptek XR-100T-CZT CdTe γ /x-ray detector was held by a laboratory clamp approximately 5 cm above ^{241}Am and ^{133}Ba sources to collect calibration spectra. The activity of the sources used was less than $1\mu\text{Ci}$. The calibration spectra are in Figures 4.5 and 4.6. Figure 4.7 is the calibration fit to the ^{241}Am and ^{133}Ba spectra peaks using the LBNL table of radioactive isotopes database [26]. With the x-ray detector attached horizontally to a laboratory stand by a laboratory clamp, spectra were collected at several distances from ports 7 and 8. Count rates were determined to allow for comparison of the spectra. In Figure 4.8, a comparison plot shows how the thick glass of the viewport at port 7 attenuated the lower energy x-rays emitted by the fusor, since only a small peak is observed around 19 keV for port 7, but a wide distribution is observed for the Mylar window of port 8, extending from almost 0 keV to 25 keV. In Figure 4.9, a comparison plot of spectra collected from port 8 at distances of 12.7 and 43.2 cm shows that at a the radiation intensity decreases as distance increases, since the same peaks are observed in both spectra, but at a lesser intensity at the 43.2 cm distance.

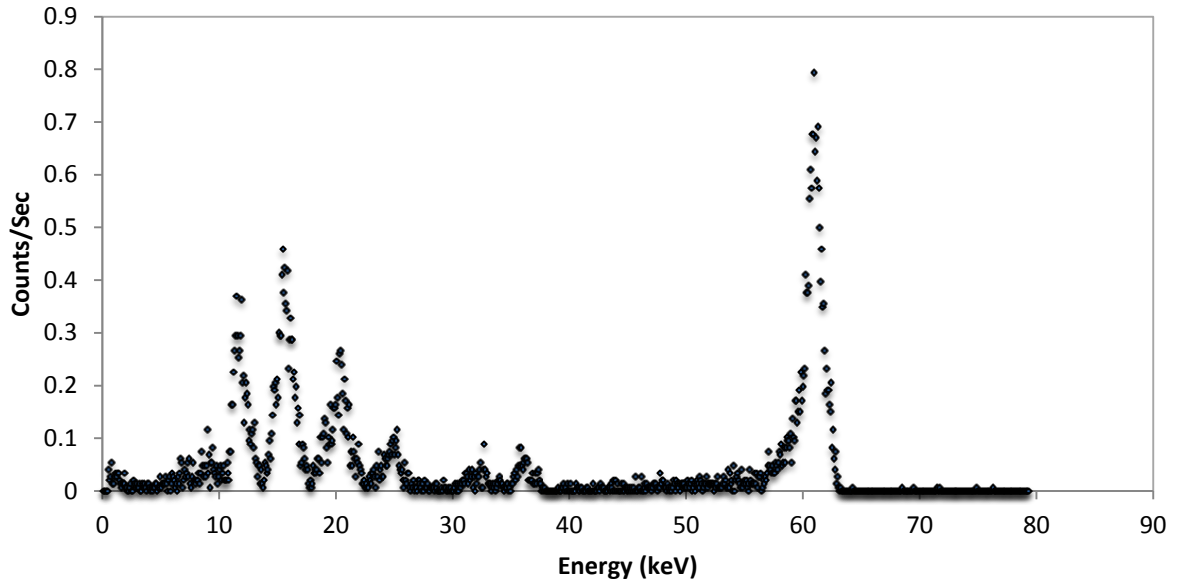


Figure 4.5 The ^{241}Am calibration x-ray spectrum, collected at 5 cm. X-ray peaks were used in the calibration fit at 14, 21, and 60 keV.

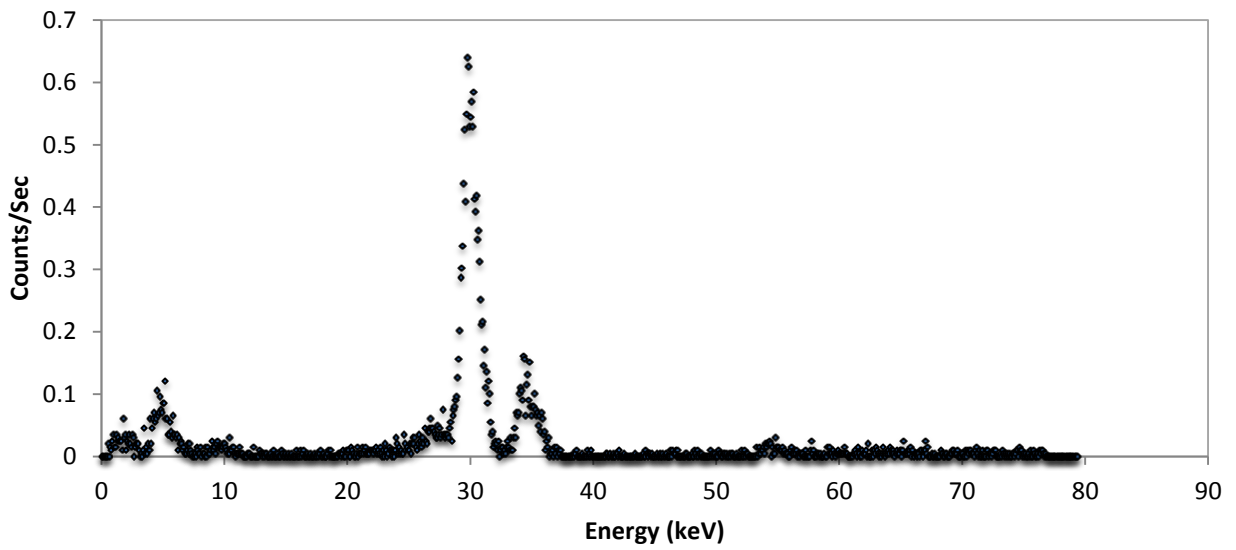


Figure 4.6 The ^{133}Ba calibration x-ray spectrum, collected at 5 cm. X-ray peaks were used in the calibration fit at 4.6, 31, and 35 keV.

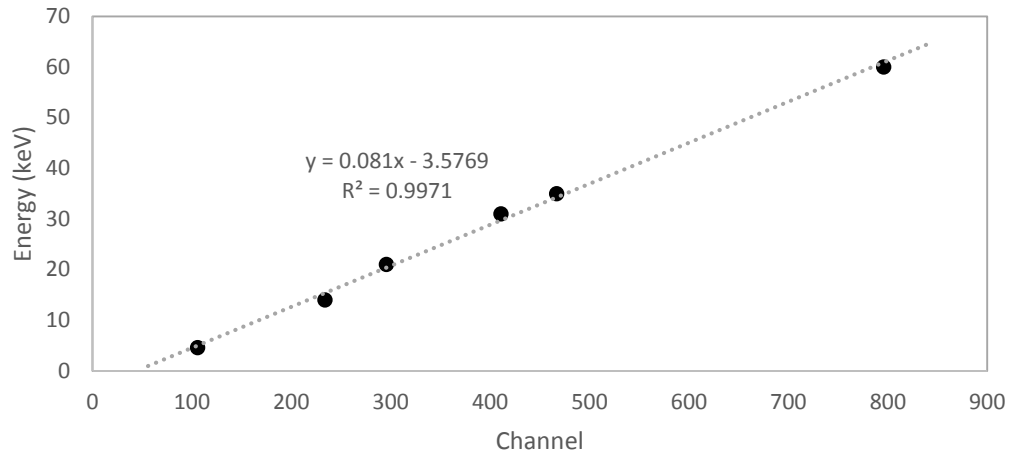


Figure 4.7 The calibration fit for the ^{241}Am and ^{133}Ba peaks.

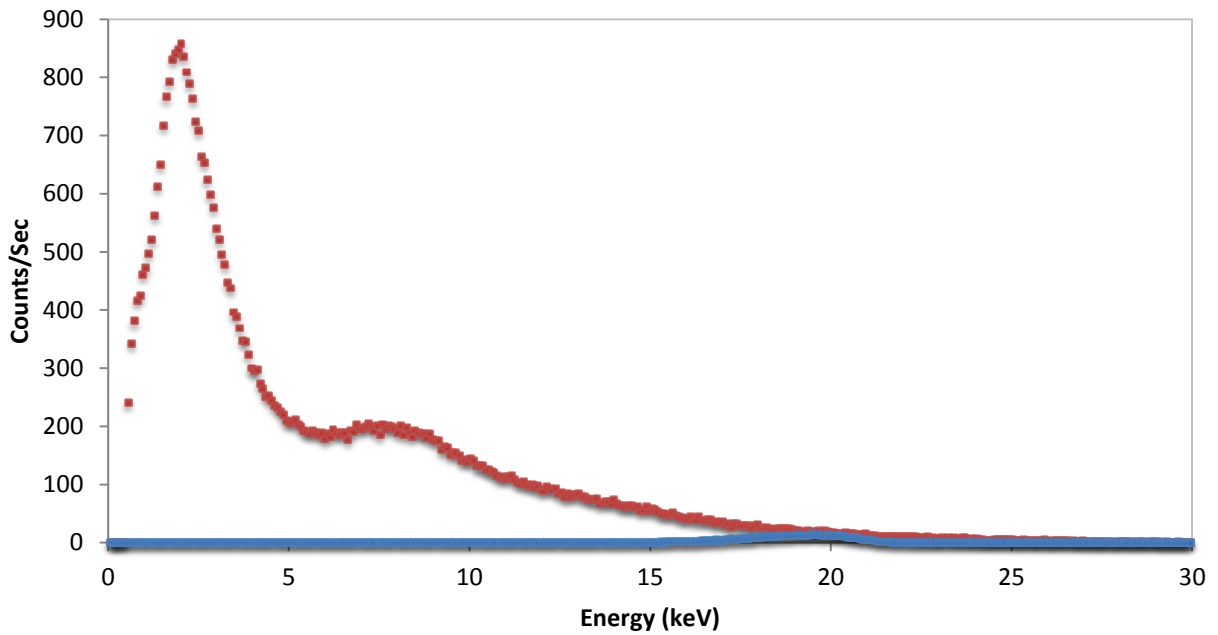


Figure 4.8 A plot comparing the spectrum (red) collected at 12.7 cm from the Mylar window of port 8 to the spectrum (blue) collected 0 cm from the thick glass window on port 7. This test was conducted at a fusor operating voltage of 25 kV. The attenuation of low-energy x-rays due to the thick glass of port 7 is observed. . The pressure was 2.3×10^{-3} Torr.

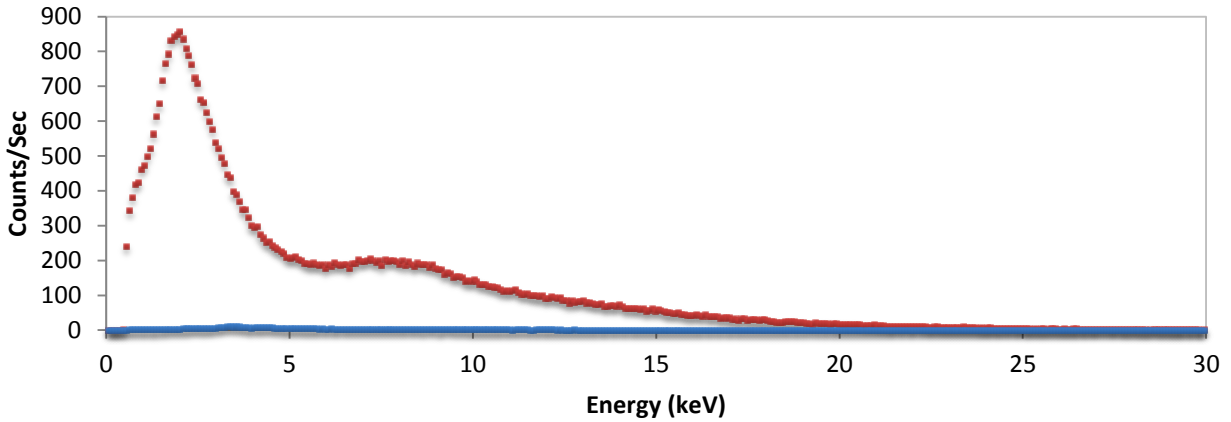


Figure 4.9 A plot comparing the spectrum (red) collected at 12.7 cm from the Mylar window of port 8 to the spectrum (blue) collected 43.18 cm from the Mylar window of port 8. This test was conducted at a fusor operating voltage of 25 kV. The decrease in intensity of radiation with distance is noticeable in the comparison of the 12.7 cm and 43.1 cm data. The pressure was 2.3×10^{-3} Torr.

4.2.3 *Photographs of Fusor operation*

During the operation of the fusor, photographs were taken to document the shape, color, and intensity of the plasma formed in the inner grid. For all tests, air was used as a source gas. Therefore, the primary color of the plasma in all photographs taken was the purple light emitted by nitrogen.

At a pressure around 1×10^{-2} Torr, as in Figure 4.10, the plasma forms closer to the high voltage electrode, and does not spread out to the spherical portion of the small grid. Once the pressure is decreased to around 1×10^{-3} Torr, the plasma spreads more out into the spherical portion of the small grid, and electron jets form, emanating from the center of the spherical part of the small electrode grid, as can be observed in Figures 4.11 and 4.12.

In Figure 4.13, the color of the plasma is more bluish, possibly due to a change in the color balance of the camera used to photograph the plasma. The shape of the plasma is still spherical, centered at the center of the small electrode grid. Multiple electron jets are observed hitting the walls of the vacuum chamber in this image.

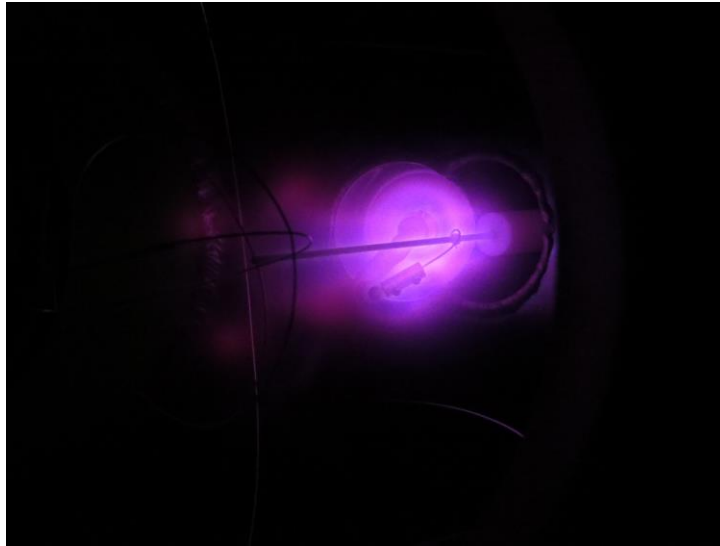


Figure 4.10 Plasma formed in air at a pressure of 1×10^{-2} Torr. The plasma has not fully moved onto the inner grid, and is located more towards the high voltage electrical feedthrough. The potential on the grid was around 10 kV and the current was approximately 1 mA.

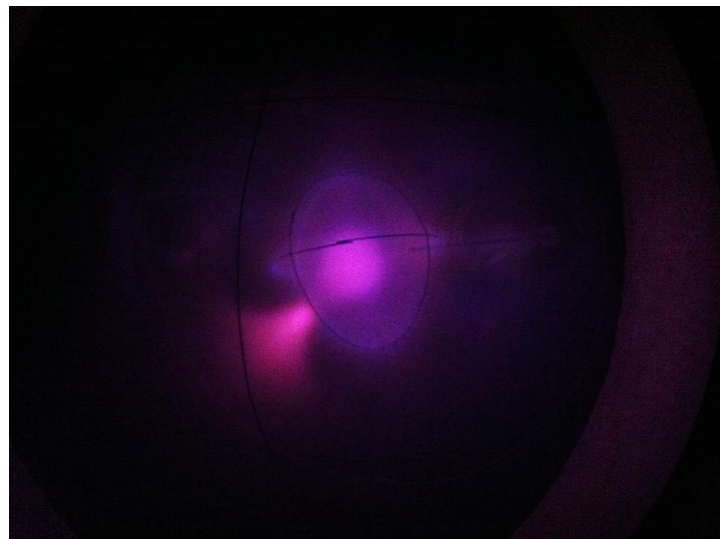


Figure 4.11 Plasma formed in air at a pressure of 1×10^{-3} Torr. Plasma density is observed in the core of the grid. Electron jets can result from irregularities in the spherical grid due to perturbations of the spherical electric field. An electron jet is seen emanating from the core of the inner electrode. The potential on the grid was around 15 kV and the current approximately 1.5 mA.

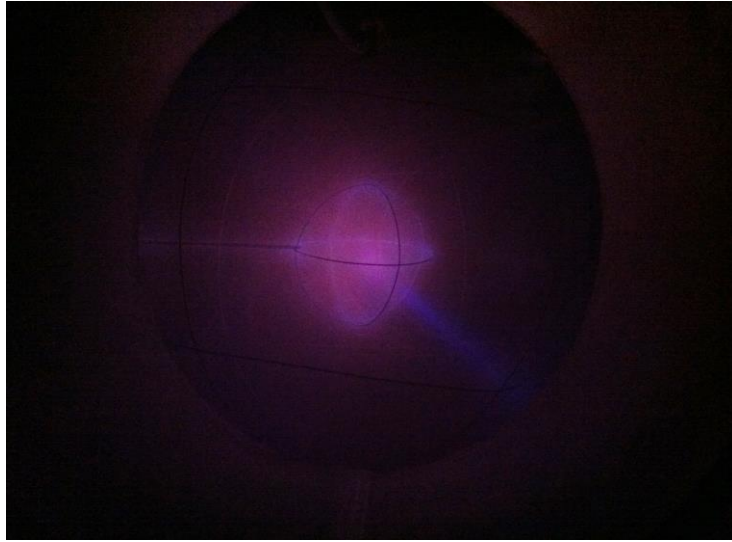


Figure 4.12 Plasma formed in air at a pressure of 1×10^{-3} Torr. An electron jet is seen emanating from the core of the inner electrode, and a smaller concentration of plasma density is observed in the core of the grid. The potential on the grid was around 18 kV and the current approximately 1.5 mA.

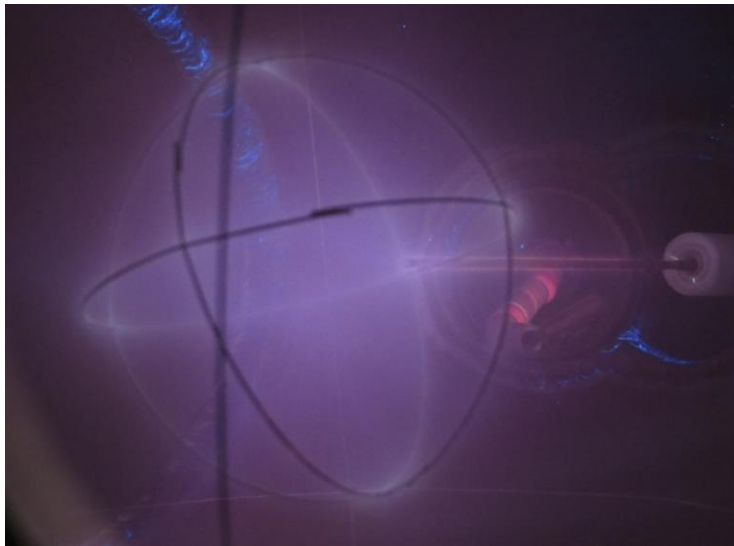


Figure 4.13 Plasma formed in air at a pressure of 1×10^{-4} Torr. The small white dots seen on the ceramic insulator at right are electron beams emanating from the core. The potential on the grid was around 23 kV and the current approximately 1.5 mA.

Chapter 5

CONCLUSIONS

5.1 **Conclusions**

A Farnsworth-Hirsch fusor has been constructed and tested for plasma formation. The vacuum system has been assembled. Electrode grids were built and placed within the vacuum chamber with necessary electrical connections to ground and the high voltage power supply. At present, the device has not been tested with source gases besides air. This device has produced plasmas at air pressures between 1×10^{-3} and 1×10^{-5} Torr with a potential of up to 29 kV on the inner grid and currents of 2 mA. Electron jets have been observed emanating from the core of the plasma in the inner grid. These electron beams strike the vacuum chamber wall, and produce bremsstrahlung x-ray radiation. Precautions were taken to place shielding on all viewports, and the Mylar window used for measuring the nearly unattenuated x-ray spectrum was surrounded by a steel collimator and covered with a steel CF flange. A CdTe x-ray detector collected x-ray emission spectra, which were analyzed to determine that the thick glass viewports remove all but the highest energies of the x-ray emission spectrum. The dose rate of the x-ray radiation produced by the fusor was measured for all ports, and at several distances from a selection of the ports.

5.2 **Future Plans**

Before proceeding with further research, remote operation and monitoring of the Farnsworth fusor will be developed for safety reasons. The Farnsworth fusor will have its pressure controlled with a mass-flow controller, so that the leak rate of the source gas into the chamber can be determined from a remote location. In addition, the pressure inside the chamber will be monitored by an InstruTech CCM501FD “Hornet” cold cathode ion gauge through an RS-485 cable connection. A computer controlled power supply will control and monitor the potential and current supplied to the grids. To further enhance radiation safety, the interlocked room doors will prevent the fusor from operating when the doors are open.

Prior to experiments with nuclear fusion, the fusor system will be tested with hydrogen gas. Then, to determine the safety of using deuterium gas as the source gas, tests with small concentrations of deuterium gas and small electrical currents will be completed. These tests will be monitored for x-ray and neutron dose rates to determine the shielding needed for safe operation. Beyond experimentation with fusion, experiments such as the investigation of the electrical properties of plasmas can be completed with the fusor device. The ability of the fusor to be used in a wide variety of experiments relating to x-ray radiation, plasmas, fusion, and other nuclear reactions ensures that future experimentation with this device.

Appendix A

PROCEDURES

A.1 Vacuum System

A.1.1 Vacuum Pump Startup Procedure

This is the procedure that is used when starting the vacuum system for operating the Houghton College Farnsworth-Hirsch type fusor. It explains how the equipment should be set up and operated to begin evacuation of the vacuum chamber.

1) Ensure that the up-to-air valves (14) and (3) are closed, and that the valve (2) between the forepump and the diffusion pump is open.

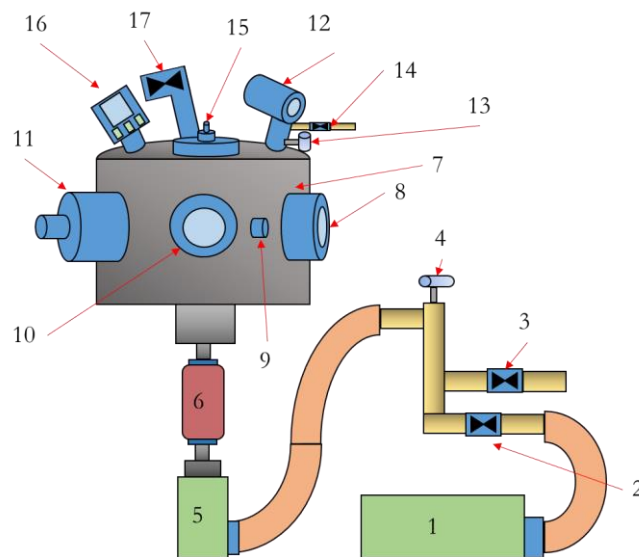


Figure A.1 In the vacuum system, the forepump (1) provides evacuation down to between 10^{-2} and 10^{-3} Torr. Valve (2) allows the forepump to pump from the chamber. The up-to-air valve (3) allows air to enter the vacuum system. A pirani gauge (4) measures the air pressure in the foreline. Pressures down to 10^{-6} Torr are obtained using the diffusion pump (5) and the cold trap (6). Ports on the vacuum chamber (7) are labeled: port 5 (8), port 6 (9), port 7 (10), and port 8 (11). A hot cathode ion gauge (12) and a pirani gauge (13) monitor the chamber pressure. The up-to-air valve (14) is attached at this site as well. Port 17 (15) contains the electrical feedthrough and linear motion feedthrough for the outer electrode grid. A CCM501 cold cathode ion gauge (16) is mounted on port 15. A variable leak valve is attached to an angle valve on port 16 (17).

- 2) Turn on the forepump (1). This turns on the diffusion pump cooling fan as well.
- 3) Wait until the pressure is around 1×10^{-3} Torr in the chamber (7), as indicated by the pirani gauge on port 12 (13).
- 4) Optionally, fill the cold trap (6) with liquid nitrogen.
- 5) Turn on the diffusion pump (5).
- 6) Check pressure as needed using the pirani gauges and the hot (12) and cold (16) cathode ion gauges. (and maintain liquid nitrogen, if used)

A.1.2 Vacuum Pump Shutdown Procedure

This is the procedure that is used when stopping the vacuum system. It explains the order in which steps must be taken to bring the system up to atmospheric pressure.

- 1) Turn off ion gauges (12) and (16).
- 2) Turn off the diffusion pump (5).
- 3) Wait about 30 minutes until the diffusion pump is cool enough to touch.
- 4) Open the up-to-air valve (14) to the chamber until a pressure of around 400 Torr is reached.
- 5) Turn off the forepump (1).
- 6) Once the pressure in the chamber has reached 760 Torr (1 atm), close all valves to prevent water vapor from entering the chamber.

A.2 High Voltage System

A.2.1 System Startup

This is the procedure for safe and proper operation of the Sorensen 230-3/12P R&D high voltage power supply. Careful detail is paid to grounding of equipment.

- 1) Check to make sure all electrical connections to the SRS IGC100 ion gauge controller are disconnected.
- 2) Make certain that the Sorensen power supply ground is attached to the vacuum chamber, which is connected to earth ground.
- 3) Make certain the Farnsworth fusor chamber is grounded to earth ground.
- 4) Check the HV electrical connection from the power supply to the resistor attached to the electrical feedthrough on the chamber.
- 5) Ensure that the Sorensen HV power supply is set to operate in the 30 kV mode, with the overload set to maximum current, and the voltage at 0 V.



Figure A.2: The Sorensen 230-3/12P R&D high voltage power supply.

- 6) Plug in the Sorensen HV power supply.
- 7) Press the “Lock” button and the “Hold” buttons at the same time to lock the power supply into operation.
- 8) Slowly dial the “coarse control” until a plasma forms and current begins to flow. If an overload occurs, reset the system, and decrease the gas pressure in the chamber. If no plasma is achieved with a potential of around 10 kV, increase the gas pressure. Repeat this process carefully until the desired pressure and potential are achieved.

A.2.2 System Reset (if an overload occurs)

If the fusor system sustains a shutdown, the server can be restarted through the use of this procedure.

- 1) Press the red “Off/Reset” button.
- 2) Return the “coarse control” dial to the zero voltage setting.
- 3) Press the “Lock” button and the “Hold” buttons at the same time to lock the power supply into operation.
- 4) Dial the “coarse control” to the desired voltage, being careful to not set off an overload.

A.2.3 System Shutdown

Once the fusor is not needed, this procedure instructs on the proper way to shut down the high voltage power supply.

- 1) Press the red “Off/Reset” button.
- 2) Unplug the Sorensen power supply from the wall socket.
- 3) If desired, reattached the previously detached SRS IGC100 ion gauge controller to power, and its appropriate sensors.

References

-
- [1] N. D. Cook, *Models of the Atomic Nucleus* (Springer-Verlag, Berlin, 2006), p. 55-57.
- [2] S. Pfalzner, *An Introduction to Inertial Confinement Fusion* (Taylor & Francis, New York, 2006), p. 2.
- [3] S. Pfalzner, *An Introduction to Inertial Confinement Fusion* (Taylor & Francis, New York, 2006), p. 3.
- [4] S. Pfalzner, *An Introduction to Inertial Confinement Fusion* (Taylor & Francis, New York, 2006), p. 9.
- [5] S. Pfalzner, *An Introduction to Inertial Confinement Fusion* (Taylor & Francis, New York, 2006), p. 10.
- [6] S. Pfalzner, *An Introduction to Inertial Confinement Fusion* (Taylor & Francis, New York, 2006), p. 11.
- [7] R Aymar et al, Plasma Phys Control. Fusion. **44** 519 (2002).
- [8] S. Pfalzner, *An Introduction to Inertial Confinement Fusion* (Taylor & Francis, New York, 2006), p. 13.
- [9] J. D. Lindl et al. Phys. Plasmas, **11** 339 (2004).
- [10] J. D. Lindl, Phys. Plasmas, **2** 3933 (1994).
- [11] G.H. Miley and S. K. Murali, *Inertial Electrostatic Confinement Fusion: Fundamentals and Applications* (Springer, New York, 2014), p. 3-4.
- [12] J. R. M. Vaughn, IEEE Trans. on Electron Devices. **35** (1988).
- [13] P. T. Farnsworth, J. Franklin Inst. **218** 411, (1934).
- [14] P.T. Farnsworth, U.S. Patent No. 2,135,615 (8 November 1938).
- [15] L. Spitzer, "Equations of Motion for an Ideal Plasma" Princeton U. Obs. (1952).
- [16] J.D. Lawson, Proc. Phys. Soc. B. **70** (1957).
- [17] W.C. Elmore, J.L. Tuck, and K.M. Watson, Phys. of Fluids. **2** 239 (1959).
- [18] P.T. Farnsworth, U.S. Patent No. 3,258,402 (28 June 1966).
- [19] R.L. Hirsch et al, U.S. Patent No. 3,530,497 (22 September 1970).
- [20] J. D. Callen, *Fundamentals of Plasma Physics*, (University of Wisconsin-Madison), WWW Document, (<http://homepages.cae.wisc.edu/~callen/chap5.pdf>), 2003. (Unpublished)
- [21] J. D. Callen, *Fundamentals of Plasma Physics*, (University of Wisconsin-Madison), WWW Document, (<http://homepages.cae.wisc.edu/~callen/chap5.pdf>), 2003. (Unpublished), pg 1.
- [22] J. D. Callen, *Fundamentals of Plasma Physics*, (University of Wisconsin-Madison), WWW Document, (<http://homepages.cae.wisc.edu/~callen/chap5.pdf>), 2003. (Unpublished), pg 2.
- [23] J. D. Callen, *Fundamentals of Plasma Physics*, (University of Wisconsin-Madison), WWW Document, (<http://homepages.cae.wisc.edu/~callen/chap5.pdf>), 2003. (Unpublished), pg 4.
- [24] J. D. Callen, *Fundamentals of Plasma Physics*, (University of Wisconsin-Madison), WWW Document, (<http://homepages.cae.wisc.edu/~callen/chap5.pdf>), 2003. (Unpublished), pg 6.
- [25] J.D. Lawson, Proc. Phys. Soc. B. **70** (1957)
- [26] LBNL, *WWW Table of Radioactive Isotopes*, WWW Document, <http://ie.lbl.gov/toi/index.asp>. (2004)